New Drosophila models to uncover the intrinsic and extrinsic factors mediating the toxicity of the human prion protein

Ryan R. Myers[1,*], Jonatan Sanchez-Garcia[2], Daniel C. Leving[1], Richard G. Melvin[1] and Pedro Fernandez-Funez[1,*]

1-Department of Biomedical Sciences, University of Minnesota Medical School, Duluth Campus, Duluth, MN 55812, USA. 2-Departent of Neurology, University of Florida, Gainesville, FL 32611, USA (Current address: Bristol-Myers Squibb, Madrid, Spain).

*Corresponding authors

Contact Information: Pedro Fernandez-Funez, PhD

Department of Biomedical Sciences,

University of Minnesota Medical School, Duluth Campus

1035 University Drive, Duluth, MN 55812

e-mail: pfernand@d.umn.edu

Phone: 218 726 6863

Keywords: Prion diseases, prion protein, Drosophila, transgenic models, protective amino acids, heat shock proteins, unfolded protein response, PERK, ATF4. suppressors

Abstract

Misfolding of the prion protein (PrP) is responsible for devastating neurological disorders in humans and other mammals. An unresolved problem in the field is unraveling the mechanisms governing PrP conformational dynamics, misfolding, and the cellular mechanism leading to neurodegeneration. The

variable susceptibility of mammals to prion diseases is a natural resource that can be exploited to understand the conformational dynamics of PrP. Here we present a new fly model expressing human PrP with new, robust phenotypes in brain neurons and the eye. Using comparable attP2 insertions, we demonstrate the heightened toxicity of human PrP compared to rodent PrP along with a specific interaction with the amyloid-β peptide. Using this new model, we started to uncover the intrinsic (sequence / structure) and extrinsic (interactions) factors regulating PrP toxicity. We describe PERK and ATF4as key cellular mechanism mediating the toxicity of human PrP and uncover a key new protective activity for 4E-BP, an ATF4 transcriptional target. Lastly, mutations in human PrP (N159D, D167S, N174S) show partial protective activity, revealing its high propensity to misfold into toxic conformations.

Introduction

Prion diseases encompass a clinically heterogeneous class of brain disorders in humans with direct molecular and pathological correlates in several mammals (Mathiason, 2017, Zlotnik and Rennie, 1965). The main pathological features shared by prion diseases are spongiform degeneration of the brain and accumulation of insoluble prion protein (PrP) (Colby and Prusiner, 2011, Scheckel and Aguzzi, 2018). PrP is a glycoprotein anchored to the extracellular aspect of the membrane not essential for survival (Sigurdson et al., 2019, Steele et al., 2007, Bueler et al., 1992). Other than humans, only ruminants suffer endemic prion diseases. Several mammals proved susceptible to transmission (chimpanzee, rodents, cattle, felines, and mustelids), while others demonstrated resistance: dogs, horses, rabbits, and pigs (Chandler, 1971, Zlotnik and Rennie, 1965, Chandler and Fisher, 1963, Zlotnik and Rennie, 1963)(Gibbs and Gajdusek, 1973, Barlow and Rennie, 1976)(Kirkwood and Cunningham, 1994, Sigurdson and Miller, 2003). These natural differences in susceptibility to prion diseases can be exploited to dissect the rules governing PrP misfolding and disease. It is likely that disease susceptibility is encoded by differences in amino acid sequence that modulate conformational dynamics without a relevant impact of the cellular milieu (Vorberg et al., 2003, Vilette et al., 2001). This knowledge can be leveraged to unravel how sequence variation (genotype) impacts PrP toxicity (phenotype) (Myers et al., 2020).

Over the last few years, we and others created transgenic *Drosophila* models expressing wild type (WT) and mutant PrP from susceptible and resistant animals: Syrian hamster, mouse, sheep, rabbit, dog, and horse (Sanchez-Garcia and Fernandez-Funez, 2018, Fernandez-Funez et al., 2010, Fernandez-Funez et al., 2009, Gavin et al., 2006, Thackray et al., 2012b, Thackray et al., 2012a). These studies support the preservation of the intrinsic properties of each PrP when expressed in flies: WT hamster, mouse, and sheep PrP are toxic in flies whereas WT rabbit, horse and dog are not. Toxicity correlates with PrP conformational dynamics, with rabbit, horse and dog PrP showing low misfolding and aggregation (Fernandez-Funez et al., 2010, Khan et al., 2010, Vidal et al., 2020, Otero et al., 2019, Erana et al., 2017, Fernandez-Borges et al., 2017). Additionally, *Drosophila* demonstrates high sensitivity to subtle changes in PrP sequence: hamster PrP is more toxic than mouse PrP (Fernandez-Funez et al., 2010), whereas dog and horse PrP carrying humanized mutations become toxic (Sanchez-Garcia and Fernandez-Funez, 2018) in progressive brain degeneration and locomotor assays. These assays are time-consuming, which dramatically narrows the utility of existing fly models. *Drosophila* is an ideal tool for cost-effective and efficient gene discovery using robust, easy to score, and sensitive assays are available, like the eye. Unfortunately, existing PrP models are not toxic in the fly eye (Fernandez-Funez et al., 2017), limiting their application.

To expand the utility of *Drosophila*, we examined whether PrP from other animals was more toxic. We hypothesized that human PrP was likely to be more toxic than PrP from other mammals with naturally occurring prion diseases (bovine, sheep, deer, moose) for the following reasons. 1) Human prion diseases, unlike other animals, present with sporadic, genetic, and infectious etiologies, arguing for higher structural instability of human PrP. 2) Human prion diseases are heterogenous brain disorders with different manifestations. Animal endemic prion diseases seem to have homogeneous presentations in each host. 3) These clinical differences can be attributed to diverse prion strains with specific neurotropisms, supporting the higher conformational dynamics of human PrP. 4) Inherited prion diseases in humans are caused by more than 50 missense mutations, some of which introduce subtle changes (e.g., V180I,

V210I). Thus, minor sequence perturbations dramatically alter human PrP dynamics. To test this idea, we generated flies expressing human PrP in a BSL3 facility to limit the risk of accumulating the transmissible, protease-resistant PrP (PrP^{res}) conformation. We showed recently that flies expressing human PrP-V129 exhibit a powerful new phenotype - small and glassy eyes - that supports the heightened toxicity of human PrP (Fernandez-Funez et al., 2017). However, we could not directly compare the toxicity of these flies against existing models expressing rodent PrP due to differences in construct design and expression levels.

Here, we describe additional novel phenotypes in the brain and in a behavioral assay induced by *random* human PrP-V129 and -M129 insertions. We also describe a new suite of comparable, isogenic transgenic flies carrying human and rodent PrP: codon-optimized and inserted in the same attP landing site (Bischof et al., 2007). These new *attP2-based* PrP models elegantly demonstrate the heightened toxicity of human PrP compared to hamster and mouse PrP. As proof-of-concept for the utility of the new human PrP model, we identified intrinsic and extrinsic factors modulating its toxicity. Accumulation of misfolded PrP in the ER triggers the unfolded protein response (UPR) (Hetz et al., 2007, Hetz et al., 2003), a complex pathway with both protective and maladaptive consequences (Hetz, 2012, Moreno et al., 2012). We describe here that PERK and ATF4 loss-of-function robustly suppress PrP toxicity, indicating that PERK is a major driver of PrP toxicity. To gain a mechanistic understanding of the sequence-structure determinants of human PrP toxicity, we introduced three protective mutations from animals resistant to prion diseases (Sanchez-Garcia and Fernandez-Funez, 2018). D167S and N174S partially suppress human PrP toxicity whereas N159D does not, illustrating the high structural stability of human PrP. These improved *Drosophila* models of proteinopathies provide expanded opportunities to identify the intrinsic and extrinsic factors mediating PrP toxicity, including high-throughput genetic screens and targeted amino acid replacements to determine the rules governing PrP toxicity.

Results

Structural differences between human and rodent PrP

The sequence alignment of the globular domain of human PrP demonstrates extensive similarity to that of hamster and mouse PrP with minor differences (Fig. S1A). All the sequences are numbered according to human PrP. Most amino acid differences between human and rodent PrP are conservative (similar chemical properties). Helix 2 and the first half of helix 3 are identical for the three sequences, whereas helix 1 displays one amino acid difference. Most variation is concentrated in the loops and the end of helix 3. The highly variable region comprised of the loop between the β-sheet and helix 2 (β2-α2 loop) forms a 3D domain with distal helix 3 (Fig. 1A). This domain is proposed to play a critical role in PrP conversion (Telling et al., 1995, Kaneko et al., 1997). For simplicity, we termed this region the C-terminal 3D (CT3D) domain (Fig. 1A). The 3D alignment of the globular domain of human and rodent PrP (Zahn et al., 2000, Calzolai et al., 2000, James et al., 1997, Riek et al., 1996) shows overt similarity (Fig. 1B and C). Mild differences may underlie their distinct toxicity. Human PrP has a longer (more stable) β-sheet than rodent PrPs despite perfect sequence conservation (Fig. 1C). Mouse PrP has a 3_{10} turn in the β2-α2 loop that indicates increased stability (Fig. 1B and C). Additionally, helix 2 starts at N173 in human PrP, Q172 in hamster PrP, and N171 in mouse PrP, resulting in a shorter helix in human PrP (Fig. 1B, arrow). Two conserved amino acids in the loop, D167 and Y169, are more exposed in human than in mouse and hamster, creating a more open loop (Fig. 1B and C). In the surface visualization of human PrP, the side chains of D167 and E168 are perpendicular to helix 3, resulting in a positive charge (Fig. S1B and E). Most animals carry D167-Q168 in the equivalent positions (Fig. S1A), resulting in a less charged domain. In mouse PrP, Q168 is upward, but the rest of the loop is lower (Fig. S1C and F). Interestingly, the loop in hamster PrP is lower and flatter than in human and mouse PrP, resulting in a closer interaction with helix 3 (Fig. S1D and G). Overall, these subtle structural differences suggest human is most unstable than rodent PrP, which informs our hypothesis.

New Drosophila eye phenotype of random human PrP insertions

A random insertion of codon-optimized human PrP-V129 induces a new eye phenotype not seen in flies expressing hamster PrP (Fernandez-Funez et al., 2017). We characterize here the toxicity of codon-optimized human PrP-V129 and -M129 from random insertions. M/V129 is a polymorphism in human PrP significant for the risk of variant Creutzfeldt-Jacob disease (CJD) transmission from cattle, but otherwise has no impact on the causation of prion diseases (Kobayashi et al., 2015). Expression of PrP-V129 and M129 resulted in disorganized, glassy eyes (Fig. 1D-F), with PrP-M129 causing a smaller eye (Fig. 1F). Semithin sections (1 μm thick) show that control flies display a regular arrangement of ommatidia, the visual units of the compound eye (Fig. 1G). Most ommatidia contain seven photoreceptors, recognized for the specialized photosensitive rhabdomeres in the center. Flies expressing human PrP-V129 have disorganized and vacuolated retinas (Fig. 1H). Most ommatidia contain fewer photoreceptors and their arrangement appears disrupted. Flies expressing human PrP-M129 show retinas with prominent disorganization and vacuolation, and few recognizable rhabdomeres (Fig. 1I). Transmission electron microscopy shows the normal polygonal arrangement of seven photoreceptors (R1-R7) around the rhabdomeres in control flies (Fig. 1J). Flies expressing PrP-V129 show rhabdomere loss and the remaining rhabdomeres are small and disorganized (Fig. 1K). One of the photoreceptors (*) appears vacuolated and others contain hyperplastic endoplasmic reticulum (ER) (Fig. 1K, arrowheads). Flies expressing PrP-M129 show few rhabdomeres and extensive vacuolation of photoreceptors (Fig. 1L, *). The rhabdomeres show low electron density and fusions. Lastly, mitochondria appear vacuolated with disrupted internal membranes (Fig. 1L, m). Overall, human PrP-V129 and M129 show robust eye perturbations affecting rhabdomere differentiation and cell survival, with characteristic vacuolar degeneration that have not been described preciously in flies expressing animal PrP.

New brain phenotypes caused by random human PrP insertions

Flies constitutively expressing human PrP under the control of the pan-neural driver *Elav-Gal4* show 100% lethality at 25˚C. In contrast, flies expressing hamster PrP under the same conditions are 100% viable. To bypass this developmental toxicity, we used the *Elav-GeneSwitch* driver (*Elav-GS*), a conditional Gal4 activated by the steroid hormone mifepristone (RU486) (Roman et al., 2001). We combined LacZ (negative control), hamster PrP, and human PrP with *Elav-GS*, and grew the flies in media lacking RU486 to allow development in the absence of PrP expression. Then, we placed newly eclosed adult flies in vials with or without RU486 at 28˚C (Day 0), and subjected the flies to climbing assays. Control experiments (- RU486) showed similar climbing ability in flies carrying LacZ, hamster PrP, or human PrP constructs (Fig. 2A). Flies expressing LacZ (+RU486) reached 50% climbing index by day 16 and climbed until day 28 (Fig. 2A). Flies expressing hamster PrP (+RU486) reached 50% climbing index at day 14 and climbed until day 26 (Fig. 2A). However, flies expressing human PrP (+RU486) reached 50% climbing index by day 1.5 and only climbed for 3 days (Fig. 2A). Differences among groups were analyzed by fitting a kinetic model and calculating area under each curve, indicating significant differences for the HuPrP+RU group (Supplementary Fig. S2 and Tables S1 and 2). The fast progression of the locomotor dysfunction illustrates the high toxicity of human PrP.

We next monitored the impact of human PrP on a brain center not critical for survival. The mushroom bodies are a well-known brain region involved in higher neural processing in insects, including memory and learning (Davis, 2005, Tanaka et al., 2008). The mushroom bodies are two symmetric centers of 2,500 neurons each with the cell bodies in the posterior brain and the axonal projections extending to the front. Expression of LacZ or hamster PrP in mushroom body neurons (*OK107-Gal4*) show robust architecture at day 1 post-eclosion (Fig. 2B and C). Notably, flies expressing human PrP from at least 12 brains lack recognizable mushroom body structures (Fig. 2D). The optic lobes are smaller due to weak expression of *OK107-Gal4* (Fig. 2D, arrowheads). Overall, these new phenotypes in the brain support our hypothesis that human PrP is more toxic than rodent PrPs. However, these phenotypes are not directly

comparable since only human PrP was codon-optimized and each construct is subjected to different position effects.

Protein analysis of random insertions of human PrP

We subjected homogenates from the heads of 1-day old flies expressing LacZ (negative control), human PrP-V129, or -M129 in the eye to western blot and detected PrP with the 3F4 antibody. M129 levels are around 4-fold higher than that for V129, possibly explaining the difference in eye phenotype (Fig. 2E). The different expression level exemplifies the problem with random insertions. We next determined whether human PrP spontaneously accumulates protease resistant PrP conformations in *Drosophila*. Transmissible prions contain PrP^{res}, which is resistant to denaturing agents and proteinase-K (PK) digestion (20 μg/ml PK for 1h at 37˚C). PK digestion of PrP^{res} results in a diagnostic PK-resistant core fragment of around 20 kDa that is transmissible. We expressed human PrP in the eye, aged the flies for 10 days, homogenized the heads, and subjected them to a mild PK gradient (2.5-15 μg/ml PK for 30 min at 25˚C) (Fig. 2F). 5 μg/ml PK eliminated full-length PrP but left fragments below 20 kDa. 7.5 and 10 μg/ml PK eliminated almost all the signal, except for small fragments around 12 and 10 kDa. Finally, 15 μg/ml PK eliminated all PrP signal. Thus, digestion under mild PK conditions demonstrate that human PrP shows no spontaneous formation of PrP^{res} in *Drosophila*.

New human and rodent PrP constructs: codon-optimized attP2 lines

To direstly compare the toxicity of human and rodent PrP, we generated a comparable suite of PrP constructs: *(a)* codon-optimized for *Drosophila* expression and *(b)* inserted in the same molecularly defined locus, the strong attP2 landing site we used before (Bischof et al., 2007, Moore et al., 2018). These new constructs enable comparative studies in which any differences in toxicity can be directly attributed to sequence differences. For human PrP, we generated the two natural polymorphisms (M129 and V129) to examine their behavior when expressed from comparable insertions. Flies expressing mouse

or hamster PrP-attP2 have normal eyes similar to those of control flies (Fig. 3A, B, C, F, G and H). Flies expressing human PrP-M129-attP2 or V129-attP2 show mild disorganization of the eye (Fig. 3D, E, I and J). Magnification shows poor differentiation of ommatidia with multiple fusions (Fig. 3I and J, arrowheads). The eye phenotype of the two human PrP-attP2 lines is, as expected, weaker than those from random insertions (Fig. 1) due to lower expression levels.

Since the human attP2-PrP constructs induce mild eye phenotypes, it could be argued that rodent PrPs could cause detectable phenotypes by pushing their expression. To test this, we generated flies carrying two copies of the PrP-attP2 constructs with one copy of *GMR-Gal4*. Flies expressing 2X mouse or hamster PrP-attP2 still exhibit normal eyes (Fig 3K, L, O and P). In contrast, flies expressing 2X human PrP-attP2 exhibit small and very disorganized eyes (Fig 3M, N, Q and R). The ommatidia have abnormal shapes and appear fused (Fig. 3Q and R, insets). Thus, doubling the expression of PrP results in qualitative differences in eye toxicity between rodent and human PrP, which supports the heightened toxicity of human PrP.

Expression analyses of the new attP2 PrP lines

We examined the mRNA expression level for the new attP2-based lines by quantitative RT-PCR (qPCR). We generated homogenates from flies expressing attP2-PrP in the eye as described above, followed by qPCR. The same primers were used for human PrP-M129 and -V129, but hamster and mouse PrP each required unique primers because of small sequence differences. After normalization to *G3PDH*, all constructs showed identical expression levels (Fig. 4A), consistent with the shared landing site at attP2.

Next, we analyzed the new PrP lines for differences in the relative accumulation of isoforms. PrP has two facultative *N*-glycosylation sites and the relative usage of these two sites depends on their availability. We generated homogenates from flies expressing mCD8-GFP-attP2 or PrP-attP2 in the eye as described above. We first used the 8H4 anti-PrP antibody that binds both human and rodent PrP. 8H4

revealed strong reactivity against human M129, hamster, and mouse PrP, but showed a weak signal for human V129 (Fig. 4B, left panel). Note that all the lanes are equally loaded as indicated by Tubulin. Quantification of three biological replicates shows that M129 accumulates at higher levels than hamster PrP ($p = 0.048$) and mouse PrP ($p = 0.121$) although mouse PrP shows more variability (Fig. 4C). V129 levels are significantly lower that all other samples. This finding was consistent over multiple replicates. It is unlikely that V129 is expressed at very low levels compared to M129 since both induce similar eye phenotypes (Fig. 3). Another possibility is that the epitope for 8H4 detects a conformational difference between the M129 and V129 polymorphisms. Unfortunately, few antibodies detect conserved epitopes in human, hamster, and mouse PrP, much less with the same affinity. We serially incubated the same membrane with 8H4 and 3F4, which does not recognize mouse PrP. 8H4 + 3F4 shows similar signal intensity and electrophoretic pattern for V129 and M129 (Fig. 4B, right panel). Both human PrPs present a strong diglycosylated isoform not present in hamster and mouse PrP, reveling differences in biogenesis.

Subcellular distribution of the new attP2 PrP lines

We next examined the subcellular distribution of rodent and human PrP to examine their transition through the secretory pathway. We co-expressed PrP-attP2 along with reporters in interneurons of the larval ventral ganglion (*OK107-Gal4*). mCD8-GFP labels plasma membrane but also stains intracellular compartments of the secretory pathway (Fig. 5A). Human PrP shows diffuse intracellular distribution extensive overlap with mCD8-GFP (Fig. 5A and B). Both rodent PrPs show punctate intracellular distribution (Fig. 5A) (Fernandez-Funez et al., 2010, Fernandez-Funez et al., 2009) with 50% overlap with mCD8-GFP (Fig. 5B). γCOPII-GFP labels 3-5 vesicles connecting the ER with the Golgi apparatus in small interneurons and more in larger neurons (Fig. 5C). Human PrP overlaps with γCOPII-GFP during its transit to the ER, but rodent PrP shows a larger overlap (Fig. 5C and D). Rab4-RFP (early endosomes) shows a few puncta per cell with some overlap with human PrP. (Fig. 5E). Rodent PrP shows more overlap with the Rab11 puncta (Fig. 5E and F). Rab11 (recycling endosomes) also accumulates in a few

puncta per interneuron in controls (Fig. 5G). Human PrP shows partial overlap with Rab11 but rodent PrP shows higher overlap (Fig. 5G and H). Lastly, Sec16-Tomato (secretory vesicles) shows diffuse expression intracellular distribution with a large vesicle close to the membrane (Fig. 5I). Human PrP shows almost complete co-distribution with Sec16 whereas rodent PrP shows around 50% overlap (Fig. 5I and J). Overall, these analyses show significant differences in the subcellular distribution of human and rodent PrP. For unknown reasons, rodent PrP is retained in several compartments of the secretory pathway whereas human PrP seems to have a smoother transition without retention in any specific vesicle.

Extrinsic modifiers of PrP toxicity: interaction of human PrP and the amyloid-β peptide

We further tested the differences between human and rodent PrP by examining genetic interactions with other factors. Multiple reports support the direct interaction of PrP and the amyloid-β42 (Aβ42) peptide in biochemical assays (Lauren et al., 2009, Chen et al., 2010, Zou et al., 2011, Gimbel et al., 2010, Gunther and Strittmatter, 2010, Balducci et al., 2010). PrP may be required for the manifestation of Aβ phenotypes in brain neurons in mouse models, suggesting a functional link between Alzheimer's and prion diseases. The new PrP-attP2 lines allowed us to test whether human and rodent PrP show similar functional interactions with Aβ42. Since high expression of Aβ42 has robust eye phenotypes (27˚C) (Casas-Tinto et al., 2011), we examined the interactions with PrP at 25˚C. As shown above, flies expressing hamster and mouse PrP-attP2 have normal eyes (Fig. S3A-C). Expression of human PrP-M129-attP2 or -V129-attP2 results in subtle disorganization (Fig. S3D and E). Co-expression of Aβ42 and GFP results in moderately disorganized eyes with a few black spots (Fig. S3F). Co-expression of hamster and mouse PrP with Aβ42 results in similar eyes to those of control flies (Fig. S3G and H). Remarkably, co-expression of human PrP-M129 or V129 with Aβ42 results in small and highly disorganized (glassy) eyes (Fig. S3I and J), demonstrating a specific functional interaction of human PrP and Aβ42.

Extrinsic modifiers of PrP toxicity: the unfolded protein response (UPR)

One of the best understood mechanisms mediating the toxicity of PrP is the accumulation of misfolded conformations in the ER, which overwhelm the folding capacity of the ER, cause ER stress, and activates the UPR (Hetz et al., 2005, Moreno et al., 2012). The UPR encompasses the coordinated activity of three ER membrane anchored sensors PERK, Ire1α, and ATF6 (Fig. S4). An increase in misfolded protein load in the ER activates the sensors and their downstream effectors. Activation of the Ire1α branch results in splicing of a 24-nt intron in the X-box binding protein 1 (XBP1) that activates XBP1s (Fig. S4). We showed previously that Aβ42 activates the XBP1-GFP sensor (Fig. 6A) (Casas-Tinto et al., 2011, Ryoo et al., 2007). Expression of human PrP-V129 also activates XBP-GFP (Fig. 6B) at levels that are significantly lower than those for Aβ42 (Fig. 6B and Table S4). In line with this, silencing Ire1α or XBP1 in flies expressing human PrP result in very small eyes (Fig. 6I-K) despite these alleles having no effect on their own (Fig. 6C-E) (Table S4). These loss-of-function results reveal the protective role of Ire1α and XBP1 in PrP toxicity. The PERK branch is the most complex because it mediates both protective and maladaptive responses (Fig. S4). Activated PERK phosphorylates eIF2α and prevents the interaction of the eIF2 complex with the ribosome, resulting in global translation inhibition and resolution of acute ER stress. Yet, chronic ER stress can result in cell death by blocking translation. To resolve acute ER stress, unconventional translation of ATF4 results in the transcriptional regulation of stress response genes and the PPP1R15 phosphatase (GADD34 in mammals). PPP1R15 dephosphorylates eIF2α to restore translation. In flies, PPP1R15 is activated by eIF2α-independent translation, like ATF4, and is not downstream of ATF4 (Malzer et al., 2013). We next examined the consequence of modulating PERK and ATF4 activity on the toxicity of human PrP. Silencing PERK or ATF4 alone has no effect in the eye (Fig. 6G and O). Remarkably, silencing PERK or ATF4 robustly suppressed PrP toxicity in the eye (Fig. 6M and U). We validated these results with multiple RNAi lines ($PEK^{KK100348}$, $PEK^{HMJ02063}$, $PEK^{GL00030}$, $ATF4^{KK111018}$, $ATF4^{JF02007}$) (Table S4). PERK overexpression in the eye alone or with PrP is pupal lethal, but adult escapers show very small eyes (Fig. 6H and N) supporting a key function of PERK

in eye development (Malzer et al., 2010). Overexpression of ATF4 alone results in slightly disorganized eyes (Fig. 6P) but combined with PrP results in very small and glassy eyes (Fig. 6V). Silencing eIF2α alone results in slight eye disorganization (Fig. 6Q) and enhanced the toxicity of PrP resulting in smaller, more disorganized, eyes (Fig. 6W). Lastly, PPP1R15 silencing alone results in slightly disorganized eyes (Fig. 6R) but causes synthetic pupal lethality with PrP using two different alleles (*PPP1R15*^{KK104106}, *PPP1R15*^{HMS00811}) (Fig. 6X). This is consistent with a significant increase in the levels of phospho-eIF2α and inhibition of protein translation. These observations indicate that phospho-eIF2α is a main driver of PrP toxicity in flies.

The robust suppression of PrP toxicity by ATF4-RNAi suggests that additional downstream effectors of ATF4 contribute to the protective activity. Recent studies have identified 4E-binding protein (4E-BP, *thor* in flies) as an ATF4 transcriptional target (Kim et al., 2020, Malzer et al., 2018, Kang et al., 2017, Vasudevan et al., 2017). Interestingly, 4E-BP binds eIF4E and prevents the assembly of the eIF4F complex, which is critical for the entry of capped mRNAs into the ribosomal small subunit. Silencing 4E-BP alone has no effect in the eye (Fig 6S) but it robustly suppresses PrP toxicity (Fig. 6Y). Flies overexpressing 4E-BP alone show no significant changes (Fig. 6T) and mildly enhance PrP toxicity (Fig. 6Z) (Table S4). These results suggest that silencing 4E-BP mediates the protective activity of ATF4, providing a second, redundant mechanism for blocking translation under ER stress.

Intrinsic mediators of toxicity: protective substitutions from animals resistant to prion diseases

Several animals are recognized for their high natural resistance to prion diseases, including dogs, horses, rabbits, and pigs (Kirkwood and Cunningham, 1994, Espinosa et al., 2020, Vidal et al., 2020, Chianini et al., 2012, Bian et al., 2017). PrP sequence shows multiple differences between these animals and human PrP; it is unclear which substitutions are protective and which are neutral (Fig. 7A). Structural studies identified residues proposed to mediate the stability of resistant PrPs: D159 in dog, S167 in horse, and S174 in rabbit and pig (Myers et al., 2020, Khan et al., 2010, Perez et al., 2010, Lysek et al., 2005).

Two of these residues are in the CT3D and D159 can impact the CT3D from a short distance (Fig. 7A). The 3D alignment of the human, dog, horse, and rabbit PrP (Fig. 7B and C) shows high overall conservation. Relevant differences include the length of the β-sheet and helix, and the CT3D domain (Fig. 7B and C). However, no clear structure-function correlation exists currently. We hypothesize that these three residues impact the dynamics of the CT3D domain in their corresponding PrPs and are responsible for the high toxicity of human PrP compared to dog, rabbit, and horse PrP.

In vivo activity of protective substitutions: eye phenotype

We previously examined the consequence of introducing the equivalent amino acid substitution from human PrP into dog, horse, and rabbit PrP. Dog PrP-D159N and horse PrP-S167D became toxic in the *Drosophila* brain neurons, whereas rabbit PrP-S174N had no effect (Sanchez-Garcia and Fernandez-Funez, 2018). To examine the mechanisms mediating human PrP toxicity, we next introduced the three protective residues from dog, horse, and rabbit PrP into human PrP-V129. We introduced N159D and D167S alone, combined (2x-N159D-D167S), or combined with N174S (3x-N159D-D167S-N174S). The N174S substitution alone is shown in a different manuscript together with Y225A (RMM and PFF, submitted). We generated transgenic flies by the same methods described above (codon-optimized and inserted in attP2) into the human PrP-V129 backbone.

Flies expressing human PrP-V129-attP2 in the eye at 27˚C exhibit slightly smaller and moderately disorganized eyes as shown before (Fig. 7D, E, J and K and Table S5). Flies expressing human PrP-N159D-attP2 show eyes similarly to those expressing V129 (Fig. 7F and L, and Table S5). Flies expressing human PrP-D167S-attP2 exhibit larger and better organized eyes than those expressing V129 (Fig. 7G and M, and Table S5). High magnification shows more definition of ommatidia, although they are abnormal (Fig. 7M, inset). Flies expressing the 2X and the 3X mutants exhibit similar organization to D167S alone (Fig. 7H, I, N and O, and Table S5), indicating no cooperative activity. Overall, these experiments show that N159D alone is not protective in the context of human PrP, whereas the reciprocal substitution in dog PrP was toxic. D167S is partially protective but shows no cooperativity with N159D

and N174S. This preliminary characterization in the eye is useful to move into more sensitive and quantitative assays in brain neurons.

In vivo activity of protective substitutions: degeneration of brain neurons

We last examined the consequence of expressing the new human PrP constructs in the mushroom bodies. Figure 8 shows the axonal projections of the mushroom body neurons, which split into dorsal (α) and medial (β and γ) lobes. We measured the surface of the projections in each genotype in young (day 1 post-eclosion) and old (day 40) flies. Control 1-day-old control flies show robust axonal projections (Fig. 8A) that expand in surface in 40-day-old flies (Fig. 8G, M and N) (Sanchez-Garcia and Fernandez-Funez, 2018, Fernandez-Funez et al., 2010). 1-day-old flies expressing PrP-V129 exhibit thinner axonal projections (Fig. 8B and M). By day 40 these flies show extensive degeneration: loss of α lobes and widespread membrane blebbing (Fig. 8H and M). 1-day-old flies expressing human PrP-N159D, D167S, 2X or 3X mutants exhibit similar axonal projections compared to young flies expressing PrP-V129 (Fig. 8C-F and M). By day 40 all the mutants show extensive blebbing, but the preservation of the lobes is different. 40-day-old flies expressing N159D show similar area to controls expressing V129 (Fig. 8I, M and N), flies expressing D167S or 2X exhibit significantly larger lobes (Fig. 8J, M and N). Flies expressing the 3X mutant show expansion of the mushroom body lobes as they age (Fig. 8L, M and N), but are still smaller than in controls. Details for the statistical analysis are shown in Table S6. Overall, the analysis of mushroom body degeneration shows that human PrP is highly toxic to brain neurons starting during development and continuing with extensive degeneration during aging, but constructs carrying the D167S substitution show moderate protection.

Discussion

Here we describe the characterization of new genetic tools in *Drosophila* with the potential to dissect the mechanism underlying PrP toxicity. We generated codon-optimized rodent and human PrP constructs and integrated them in the same attP2 landing site. Since two copies of rodent PrP induce no eye toxicity, it is unlikely that higher expression levels alone are responsible for the new phenotypes of human PrP. Instead, it is likely that human PrP acquires conformations responsible for their high toxicity in flies. Differences in the biogenesis of rodent and human PrP are evidenced by different glycosylation patterns and subcellular distributions. PrP glycosylation isoforms indicate different exposure of the glycosylation sites. Retention of rodent PrP in the secretory pathway indicates slow or inefficient maturation resulting in reduced membrane expression. Previous studies showed that hamster PrP accumulates no immature glycosylation and presence in lipid rafts (Fernandez-Funez et al., 2010, Fernandez-Funez et al., 2009), suggesting that rodent PrP can complete its maturation and secretion. The partial retention in the secretory pathway may result in some degradation, explaining the higher protein levels of human PrP despite identical levels of mRNA. In addition to the eye phenotype, human PrP induces other novel phenotypes: lethality, aggressive locomotor dysfunction, and elimination of the mushroom bodies. Importantly, human PrP is sensitive to mild PK digestion, indicating no accumulation of spontaneous PrP^{res}. Flies are not expected to generate prions spontaneously just like WT or transgenic mice do not develop prions spontaneously. Transmissible prions require specific structural properties that can be replicated from seeds but are rarely produced *de novo* in humans and some ungulates, and require extensive incubation. Other labs have reported the ability of flies to replicate mammalian prion seeds in transmission experiments, demonstrating a good cellular environment for PrP conversion (Thackray et al., 2014, Thackray et al., 2012a). The lack of spontaneous PrP^{res} is consistent with the idea that neurotoxicity is caused by a different conformations from transmissible PrP (Sandberg et al., 2014, Sandberg et al., 2011). The lack of spontaneous PrP^{res} in flies suggests that responsible work can be done with these flies at enhanced Animal Biosafety Level 2 (ABSL2).

As a proof-of-concept for the sensitivity of these flies to extrinsic factors modulating PrP toxicity, we examined the functional interaction of human PrP with Aβ42 and the UPR. In 2009, Aβ42 was found to bind the unstructured N-terminal domain of PrP, a novel interaction proposed to mediate Aβ42-dependent inhibition of long-term potentiation (Lauren et al., 2009). Despite initial resistance (Calella et al., 2010, Kessels et al., 2010, Balducci et al., 2010), the interaction was confirmed by different techniques, although studies still disagree on the functional meaning of this interaction (Chen et al., 2010, Zou et al., 2011, Gimbel et al., 2010, Gunther and Strittmatter, 2010, Balducci et al., 2010). The native PrP conformation is proposed to work as a scaffold that brings together membrane proteins in lipid rafts, including glutamate and lamin receptors (Zhang et al., 2019). The Aβ42 – PrP interaction stimulates glutamate receptors whereas the interaction with lamin receptors internalizes the complexes, resulting in significant ER stress by retrograde transport of Aβ42 (Casas-Tinto et al., 2011). Here, we show that human PrP, but not hamster or mouse PrP, increases Aβ42 toxicity. This is consistent with our finding that human PrP has more binding sites for Aβ42 (six) than mouse PrP (one) (Zou et al., 2011). Additionally, Aβ42 and human PrP induce similar, although not identical, eye phenotypes in flies suggesting that Aβ42 and PrP perturb similar gene networks in the eye, including ER stress.

Our analysis of the UPR showed that silencing Ire1α or XBP1 robustly enhance PrP toxicity, indicating the protective activity of this pathway. Surprisingly, XBP1 overexpression has no effect on PrP toxicity. XBP1 is expected to show protective activity because its downstream targets support ER proteostasis. In our previous work we showed that XBP1s overexpression is protective in flies expressing Aβ42 (Casas-Tinto et al., 2011). XBP1 also shows protective activity against other stressors in *C elegans* (Taylor and Dillin, 2013). A general assumption is that all UPR branches are equally responsive and protective against all triggers. We show here that human PrP activates the Ire1α branch in flies, yet Aβ42 induces a stronger response. This is consistent with our previous findings that cultured cells exposed to oligomeric amyloids, with Aβ42 and α-Synuclein induce stronger activation of Ire1α than the PrP106-126 fragment and the British amyloid peptide (Castillo-Carranza et al., 2012). Thus, human PrP may be

only a moderate inducer of the Ire1α branch while robustly inducing the PERK branch. Notably, this robust PERK activation shuts down translation through phospho-eIF2α, thus preventing the transcriptional response of XBP1.

Our main finding is that silencing either PERK or its effector ATF4 robustly suppress human PrP toxicity. This robust protective activity is consistent with recent findings in prion infected mice (Hughes and Mallucci, 2019, Moreno et al., 2012). We report here for the first time a similar protective activity of ATF4, indicating that modulating ATF4 activity elicits a full protective activity equivalent to silencing the upstream sensor. Moreover, increased PERK or ATF4 activity perturbs the eye, but only ATF4 shows a strong genetic interaction with PrP since PERK disrupts eye development on its own. The robust ATF4 interactions with PrP are surprising since the PERK maladaptive activity is proposed to emanate from the phospho-eIF2α, a direct PERK target. It is prudent to remember that the PERK pathway is slightly different in flies and mammals. Flies do not express a CHOP orthologue, which is an ATF4 target with deleterious activities, eliminating CHOP as the effector of ATF4 toxicity in flies. Additionally, in flies PPP1R15 is activated directly by PERK by the same translational mechanism as ATF4 (Kang et al., 2015). We show here that 4E-BP, an ATF4 target discovered in the Gcn2 (General control non-repressible 2) nutrition-sensing pathway (Kim et al., 2020, Malzer et al., 2018, Kang et al., 2017, Vasudevan et al., 2017), is also involved in PrP toxicity. eIF2α is a key regulator of translation that is activated by PERK, Gcn2 and two additional kinases and eIF2α downstream effectors are likely shared by the stress pathways. Thus, the ATF4 transcriptional target 4E-BP is activated in flies expressing human PrP and resulting in chronic blocking of translation by binding to eIF4E. It is likely that the sequential activity of phospho-eIF2α and 4E-BP produce a robust translational inhibition to ensure recovery from ER stress or nutritional deficiency. Silencing 4E-BP suppresses PrP toxicity by allowing translation to proceed, but is expected to have no impact on the levels of phospho-eIF2α, which can still block translation. Since phospho-eIF2α can be rapidly dephosphorylated by PPP1R15, removing 4E-BP

can achieve robust suppression of PrP toxicity on its own despite being downstream of phospho-eIF2α. We will further investigate the interplay between PERK, Gcn2, ATF4, eIF2α, and 4E-BP in follow up studies.

We do not yet fully understand the exact intrinsic mechanisms mediating the conformational dynamics of PrP and how they translate into different toxicity, disease susceptibility, or strain variability. While a few amino acid differences between mammalian PrPs are responsible for conformational differences, it remains challenging to pinpoint how specific amino acids contribute to PrP conformation (Myers et al., 2020). The new *Drosophila* models enable mechanistic studies into sequence-structure-phenotype analyses through the efficient introduction of candidate mutations into the human PrP backbone. In a previous report we showed that two humanized mutants, dog PrP-D159N and horse PrP-S167D, turned toxic these non-toxic PrPs (Sanchez-Garcia and Fernandez-Funez, 2018). We predicted that the corresponding protective residues from dog and horse PrP into human PrP would be protective. D167S is mildly protective in the eye and the mushroom bodies yet N159D only shows weak protection of mushroom body neurons. Interestingly, the combinations N159D-D167S or N159D-D167S-N174S showed similar protective activity as D167S alone. These results provide valuable lessons about the rules governing PrP misfolding and toxicity. First, single amino acid changes are not enough to alter the high structural dynamics of human PrP. Second, N159D and D167S are not known to form distinct secondary or tertiary structures in dog and horse PrP (Perez et al., 2010, Lysek et al., 2005), suggesting that they do not introduce significant changes in human PrP. In contrast, S174 participates in a helix-capping domain that stabilizes helix 2 in rabbit PrP (Khan et al., 2010). However, addition of N174N to the 3X mutant had a small effect. Third, combining amino acid changes from different animals did not increase the conformational stability of human PrP. A more likely strategy would consist of combining conservative changes *from the same animal* to recreate local structural features from dog, horse, or rabbit PrP. We are currently testing several such combinations, including Y225A from rabbit (PFF, submitted) and others.

The ability to efficiently test candidate mutations *in vivo* will eventually provide answers to the questions posed above about the genotype - morphotype - phenotype correlations.

Materials and Methods

Sequence alignment and 3D protein visualization

The alignments of the globular domain of human, hamster, mouse, dog, horse, and rabbit prion protein sequences was done using ClustalW2 (www.ebi.ac.uk/Tools/clustalw2). We used human PrP as reference and amino acid numbering for all species refers to the corresponding amino acid in human PrP (see Fig. 1A). Amino acid sequences were obtained from NCBI with the following accession numbers: AAH22532 (human), B34759 (Syrian hamster), and AAA39996 (mouse), AAD01554 (rabbit), ACG59277 (horse), and ACO71291 (dog). The color-coded amino acids indicate properties relevant for protein structure (size and charge). To generate 3D views of human, mouse and Syrian hamster PrP, we opened in PyMOL (pymol.org) the published NMR structures for human (1QM2), mouse (1XYX), hamster (1B10), rabbit (2FJ3), horse (2KU4), and dog (1XYK) PrP deposited in the RSCB Protein Data Bank (rcsb.org/pdb). We displayed the proteins in Cartoon formats showing only relevant amino acids to optimize their visualization. We also displayed the β2-α2 loop using the Surface and Mesh views.

Generation of transgenic flies and genetics

Random insertions: Flies carrying the human PrP-WT (V129) construct in a random insertion were described previously (Fernandez-Funez et al., 2017). We generated flies carrying human PrP-M129 in a random insertion following the same procedures described above. attP2 insertions: The constructs carrying human PrP-M129, human PrP-V129, hamster PrP-WT, and mouse PrP-WT, and the human PrP mutants human PrP-N159D, -D167S, -N159D-D167S (double), and -N159D-D167S-N174S (triple, 3X) (all in V129 background) were chemically synthesized by Integrated DNA Technologies (IDT) using codon-optimized sequences for *Drosophila*. Assembled sequences were cloned between *XhoI* and *Xba*I sites onto the pJFRC7-20XUAS-IVS-mCD8:GFP *Drosophila* expression vector (Addgene #26220,

(Pfeiffer et al., 2010)) after removing the mCD8:GFP transgene. The final constructs were sequenced to verify their integrity. The pUAST-based constructs were injected into *yw* embryos at Rainbow Transgenics following standard procedures (Rubin and Spradling, 1982) to generate multiple independent transgenic lines for each plasmid. Two independent strains were generated for each construct since they are all inserted in the same attP locus.

The driver strains *GMR-Gal4* (retina, all eye cells) (Mathew Freeman, Univ. of Oxford), *OK107-Gal4* (mushroom bodies) (Connolly et al., 1996), *Elav-Gal4* (pan-neural) (Lin and Goodman, 1994), *Elav-GS* (pan-neural, GeneSwitch) (Roman et al., 2001), the reporters *UAS-LacZ UAS-mCD8-GFP, UAS-Rab4-RFP, Rab11-GFP, Sec16-Tomato and γCOPII-GFP*; the TRiP RNAi lines *Ire1α*^{HMC05163}, *XBP1*^{JF02012}, *PEK*^{HMJ02063}, *crc/ATF4*^{JF02007}, *eIF2α*^{GLC01598}, *PPP1R15*^{HMS00811}, and *Thor*^{HMS06007} *(4E-BP); and UAS-PERK* (*pek*), *UAS-ATF4* and *UAS-Thor* were obtained from the Bloomington Drosophila Stock Center (fly.bio.indiana.edu). RNAi alleles for *PERK*, *ATF4*, *PPP1R15*, and *eIF2α* were obtained from the Vienna Drosophila Stock Center (stockcenter.vdrc.at/control/main) (see Table S4). Transgenic flies expressing human Aβ42 and UAS-mouse XBP1s were described previously (Casas-Tinto et al., 2011) and the *XBP-GFP* sensor was obtained from HD Ryoo (Ryoo et al., 2007). UAS alleles for *ATF4*, *eIF2α,* and *PPP1R15* were obtained from FlyORF (flyorf.ch/index.php). Fly stocks were maintained on standard *Drosophila* medium at 25°C. For experiments, homozygous females for the *Gal4* strains were crossed with *UAS* males to generate progeny expressing *PrP* in the desired tissue. Crosses were placed at 25°C for two days, transferred to 27°C until the progeny completed development, and adults were aged at 27°C, unless otherwise indicated.

Characterization of eyes

We expressed all the constructs in the eye under the control of *GMR-Gal4*. Crosses were performed at 25˚C for 2 d and the progeny were raised at 28˚C, and adult flies were collected at day 1. Images are collected from flies with representative phenotypes out of large progenies of more than 10 females. To image fresh eyes, we froze the flies at -20˚C for at least 24 h and collected images as z-stacks with a Leica Z16 APO using a 2X Plan-Apo objective. Flattened in-focus images were produced with the Montage Multifocus module of the Leica Application Software. Fresh eyes were scored for changes with respect controls: N-no change, E-enhancer, S-suppressor. Changes in the eyes were also scored in 4 categories from 0-3 in each: eye size, organization, pigmentation and lethality. 0-no change, 3-maximum change. Changes were assessed from large progenies (at least 10 flies) and scores reflect representative and highly reproducible changes. For scanning electron microscopy, flies were serially dehydrated in ethanol, critically dried, and metal-coated for observation in a Jeol JSM-6490LV. For transmission electron microcopy, we collected flies of the appropriate genotype 1-day post eclosion, fixed the heads in 3% glutaraldehyde overnight, washed in phosphate buffer, post-fixed in 1% OsO4, dehydrated in ethanol and propylene oxide, embedded in resin, and subsequently mounted the heads in molds as described previously (Fernandez-Funez et al., 2000). Blocks were then cut into semithin sections (1 μm), stained with toluidine blue and imaged in a Nikon Eclipse Ni microscope with a 100x Plan Apo oil 1.4 NA objective. For ultrastructural analysis of the eyes, we collected ultrathin sections (70 nm), stained the sections, and imaged the samples between 2,500 and 25,000x magnifications using a Jeol JEM-1400PLUS TEM at the University Imaging Centers.

Drosophila homogenates and western blot

Ten flies per genotype and time point were used for analysis. Fly heads were homogenized in 30 μl of RIPA buffer containing Complete protease inhibitors (Roche) using a motorized pestle and centrifuged for 1 min at 1,000 rpm. 25 μl of supernatant was mixed with loading buffer and resolved by SDS-PAGE in 4-12% Bis–Tris gels (Invitrogen) under reducing conditions and electro-blotted onto nitrocellulose

membranes. Membranes were blocked in TBS-T containing 5% non-fat milk and probed against the primary antibodies: anti-PrP clone 8H4 (1: 10,000, Millipore, batch 099M4844V), anti-PrP clone 3F4 (1: 10,000, Millipore, Lot 3150381), anti-β-Tubulin (1: 50,000, Invitrogen, clone 2 28 33). The secondary antibody was anti-Mouse-HRP (1: 4,000) (Jackson ImmunoResearch, Lot 138817). Antibodies were validated by using control lanes (non-PrP) and verification of expected profile. Immunoreactive bands were visualized by enhanced chemiluminescence (ProSignal Dura ECL, Genesee). The protein biochemistry protocols are described in more detail in (Sanchez-Garcia et al., 2013). For the protease-resistance assay, fly brain homogenates were incubated with PK concentrations from 0 to 15 μg/ml for 30 min at 25°C. The digestions were stopped by adding 2mM PMSF and analyzed by western blot by staining with the 3F4 antibody. For quantitation of signal intensity, film was scanned at high resolution and the bands were measured for intensity, normalized for background, internal control, graphed in Excel, and analyzed by two sample T-Test.

Quantitative RT-PCR (qPCR)

Ten male flies 1-2 days post eclosion were used per genotype for analysis. Fly heads were homogenized in 100 μl RTL buffer from RNeasy kit (Qiagen) using a motorized pestle. An additional 250 μl RTL buffer were added and then centrifuged for 3 minutes at 14,000 rpm. Supernatant was collected, placed in a new tube, and used for RNA extraction using the RNeasy kit. Additional DNase (DNase I, NEB) treatment and ethanol precipitation was performed. Omniscript Reverse Transcription Kit (Qiagen) was used for cDNA synthesis, following the manufacturers protocol and using 50 ng RNA for each sample. cDNA was then diluted 5x before qPCR.

qPCR was performed on a Roche Lightcycler 480 Instrument II and using SYBR Green I Master Mix (Roche), following the manufacturers protocol. PrP primers were designed to amplify the same sequence. The housekeeping *Drosophila* gene *Glyceraldehyde 3-phosphate dehydrogenase* (*GAPDH*) was used as an internal control. Negative RT controls were run to eliminate contaminating genomic DNA. The

following primers were used: Human PrP forward- GCGGCAATCGTTACCCTCCTC; Human PrP reverse- ACTGGGCTTATTCCACTGGGAGT; mouse PrP forward- GTAACCGCTACCCACCGCAAG; mouse PrP reverse- TGGTTTGCTGGGCTTGTTCCA; hamster PrP forward- TCCCCAGGAGGTAATCGGTATCCT; hamster PrP reverse- TGGTTATGAGTGCCTCCACCCT; GAPDH forward- TAAATTCGACTCGACTCACGGT; GAPDH reverse- CTCCACCACATACTCGGCTC. Each genotype was examined in three biological replicates along with three technical replicates for each. The -ΔΔct method was used for data analysis and represented as the relative expression to human PrP.

Immunofluorescence, microscopy, image display, and analysis

Whole-mount immunohistochemistry of fixed larval brains or eye imaginal discs was conducted by fixing in 4% formaldehyde, washing with PBT, and blocking with 3% bovine serum albumin before incubating with the primary antibody as described previously (Fernandez-Funez et al., 2010). We incubated first with the 8H4 anti-PrP antibody (1: 2,000 dilution) followed by the secondary antibody anti-mouse-Cy3 (Molecular Probes) at 1:1,000 dilution. We mounted the stained tissues in Vectashield antifade (Vector) mounting medium for microscopic observation and documentation. We collected fluorescent images in an LSM 710 Zeiss confocal system using 10X NA: 0.45 (air), 20X NA: 1.0 (air), and 63X NA: 1.4 (oil) objectives in thick samples as Z-stacks. All genotypes for the same experiment were imaged with the same settings. From the Z-stacks, we created maximum intensity projections or extracted single planes images using the Zeiss Zen software. These images were combined into figures using Adobe Photoshop; processing included trimming of non-informative edges and brightness / contrast adjustment to whole images. The cartoon for the UPR pathway was created in Adobe Illustrator. Whole-mount adults brains labeled with mCD8-GFP were imaged at day 1 post-eclosion with the 10X objective.

Subcellular localization: We co-expressed the *PrP* constructs along with *mCD8-GFP, UAS-Rab4-RFP, Rab11-GFP, Sec16-Tomato and γCOPII-GFP* in interneurons of the larval ventral ganglion under the control of *OK107-Gal4* (*UAS-reporter-GFP; OK107-Gal4 / UAS-PrP*). Regions containing interneurons were imaged with a 63X objective and 1.5X digital zoom. Images displayed in the figure are representative single planes extracted from the stacks. For the analysis of overlap, we created the maximum intensity projections, obtained the signal intensity for 20-30 individual cells before and after subtracting the signal for both channels, normalized the signal for the surface (neuron size) and calculated the fraction of overlap to total. Differences between rodent and human PrP were calculated by T-test. For CD8-GFP-GFP, mouse and hamster PrP were statistically comparable and were aggregated to compared to both human PrPs.

XBP-GFP: Eye imaginal discs expressing XBP-GFP in the eye under the control of GMR-Gal4 were combined with LacZ, Aβ42 or PrP. Imaginal discs were imaged with the 20X objective. Signal intensity for flattened images was extracted in Adobe Photoshop 2021 following manual outlining of the anterior region of the eye disc. Oneway ANOVA analysis was conducted in JMP Pro 16. Following the finding that the averages were statistically significant, we performed a Tukey-Kramer post hoc pair-wise analysis of significance to determine which pairs were statistically different while reducing the false positive due to the analysis of multiple pairs. To simplify the multiple group comparisons, we displayed the connecting letters report: groups with different letters correspond to statistically significant differences, with the differences being proportional to the distance between the letters. See details in Supplementary Table S3.

Mushroom body degeneration: We crossed *OK107-Gal4; mCD8-GFP* flies with *LacZ* alone (negative control) or with *PrP* constructs (*UAS-mCD8-GFP; OK107-Gal4/UAS-PrP*) at 27˚C. Adult flies were collected at days 1 and 40 post eclosion and imaged with the 63X objective. The surface for mushroom body axonal projections was manually outlined and measured in Photoshop from 15-20 mushroom bodies. Image analysis data was exported to Excel to calculate averages, standard deviations and create

graphs. Two-way ANOVA analysis of the effects of genotype and age was conducted using JMP Pro 16. ANOVA showed significant effects of genotype ($F_{5, 121} = 106.79$, $p < 0.001$), age ($F_{1, 121} = 5.32$, $p < 0.05$) and the interaction of genotype with age ($F_{5, 121} = 48.35$, $p < 0.001$). Following ANOVA, *post hoc* pairwise t-test analyses were conducted in JMP Pro 16. T-tests were corrected using Holm's method (Sokal and Rohlf, 2012).

Behavior, locomotor assays

For the strong random human PrP insertion, we performed locomotor assays following conditional expression in adult flies with the Elav-GS system. For this, we combined *Elav-GS* with *UAS-LacZ*, *UAS-hamster PrP-random*, and *UAS-human PrP-random* and placed the crosses in fly media without the activator RU486 (Sigma). When the adult flies eclosed, we collected 20 females per replicate and split them in two groups: one in vials without RU486 and one with RU486. Then, we examined the ability to move vertically in an empty vial (climbing assay) at 28°C (Le Bourg and Lints, 1992). Briefly, 20 newborn adult females were placed in empty vials in duplicate and forced to the bottom by firmly tapping against the surface. After 10 sec, the number of flies that climb above 5 cm was recorded. This was repeated 8 times to obtain the average climbing index each day. At the end of the assay, the climbing index (flies above line/total flies x 100) was plotted as a function of age in Excel.

Climbing index data were fit to either a 3-parameter logistic (LacZ ± RU, HaPrP ± RU, and HuPrP − RU) or 3-parameter first order decay kinetic model (HuPrP + RU) using JMP Pro 16 (SAS Institute). Fitted curves were used to predict the time in days to climbing index values (age-specific climbing index) of 90, 75, 50, 25, and 10 ($\alpha = 0.05$) (Table S1). Prediction using increasingly more stringent α values did not change the prediction. Prediction formulas and parameters for each genotype-RU combination are listed in Table S2. We tested the null hypothesis that RU had no effect on age-dependent climbing ability using a single sample t-test. Single-sample t-test with 5 degrees of freedom (critical value = 2.015 at $\alpha = 0.05$) showed a significant negative effect of RU on age-dependent climbing

effect when combined with HuPrP. We calculated t-scores instead of z-scores because sample size was ≤ 30. Additionally, we computed the area under each climbing index curve. Single-sample t-test again confirmed a significant negative effect of the HuPrP + RU combination on climbing index.

Acknowledgements

We thank the Bloomington Drosophila Stock Center (NIH P40OD018537), the Vienna Drosophila Stock Center, and FlyORF, HD Ryoo for transgenic flies; the RSCB Protein Data Bank and ClustalW2, for free data and software; and the University of Minnesota Information Technology Support Services for institutional copies of PyMOL, Adobe 2021 products and JMP Pro 16. This work was supported by the resources and staff at the University of Minnesota Imaging Centers (SCR_020997). Gail Celio assisted with sample preparation and TEM imaging of the eyes. This work was supported by the NIH grant 7R21NS096627-02 and the Winston and Maxine Wallin Neuroscience Discovery Fund award CON000000083928 to PF-F. Confocal and SEM images were collected at the Research Instrumentation Laboratory (UMN-UMD).

Competing Interests: The authors declare that no competing interests exist.

Author contributions: PFF conceived the study; RM, JSG, DL and PFF performed experiments; RM, JSG, DL and PFF interpreted the experiments; PFF, RM and RGM performed statistical analyses. RM, DL and PFF wrote the manuscript. All authors revised and approved the final manuscript.

References

BALDUCCI, C., BEEG, M., STRAVALACI, M., BASTONE, A., SCLIP, A., BIASINI, E., TAPELLA, L., COLOMBO, L., MANZONI, C., BORSELLO, T., CHIESA, R., GOBBI, M., SALMONA, M. & FORLONI, G. 2010. Synthetic amyloid-beta oligomers impair long-term memory independently of cellular prion protein. *Proc Natl Acad Sci U S A*, 107**,** 2295-300.

BARLOW, R. M. & RENNIE, J. C. 1976. The fate of ME7 scrapie infection in rats, guinea-pigs, and rabbits. *Res. Vet. Sci.*, 21**,** 110-111.

BIAN, J., KHAYCHUK, V., ANGERS, R. C., FERNANDEZ-BORGES, N., VIDAL, E., MEYERETT-REID, C., KIM, S., CALVI, C. L., BARTZ, J. C., HOOVER, E. A., AGRIMI, U., RICHT, J. A., CASTILLA, J. & TELLING, G. C. 2017. Prion replication without host adaptation during interspecies transmissions. *Proc Natl Acad Sci U S A*, 114**,** 1141-1146.

BISCHOF, J., MAEDA, R. K., HEDIGER, M., KARCH, F. & BASLER, K. 2007. An optimized transgenesis system for Drosophila using germ-line-specific phiC31 integrases. *Proc Natl Acad Sci U S A*, 104**,** 3312-7.

BUELER, H., FISCHER, M., LANG, Y., BLUETHMANN, H., LIPP, H. P., DEARMOND, S. J., PRUSINER, S. B., AGUET, M. & WEISSMANN, C. 1992. Normal development and behaviour of mice lacking the neuronal cell-surface PrP protein. *Nature*, 356**,** 577-82.

CALELLA, A. M., FARINELLI, M., NUVOLONE, M., MIRANTE, O., MOOS, R., FALSIG, J., MANSUY, I. M. & AGUZZI, A. 2010. Prion protein and Abeta-related synaptic toxicity impairment. *EMBO Mol Med*, 2**,** 306-14.

CALZOLAI, L., LYSEK, D. A., GUNTERT, P., VON SCHROETTER, C., RIEK, R., ZAHN, R. & WUTHRICH, K. 2000. NMR structures of three single-residue variants of the human prion protein. *Proc Natl Acad Sci U S A*, 97**,** 8340-5.

CASAS-TINTO, S., ZHANG, Y., SANCHEZ-GARCIA, J., GOMEZ-VELAZQUEZ, M., RINCON-LIMAS, D. E. & FERNANDEZ-FUNEZ, P. 2011. The ER stress factor XBP1s prevents amyloid-beta neurotoxicity. *Hum Mol Genet*, 20**,** 2144-60.

CASTILLO-CARRANZA, D. L., ZHANG, Y., GUERRERO-MUNOZ, M. J., KAYED, R., RINCON-LIMAS, D. E. & FERNANDEZ-FUNEZ, P. 2012. Differential activation of the ER stress factor XBP1 by oligomeric assemblies. *Neurochem Res*, 37**,** 1707-17.

CHANDLER, R. L. 1971. Experimental transmission of scrapie to voles and Chinese hamsters. *Lancet*, 1**,** 232-3.

CHANDLER, R. L. & FISHER, J. 1963. Experimental Transmission of Scrapie to Rats. *Lancet*, 2**,** 1165.

CHEN, S., YADAV, S. P. & SUREWICZ, W. K. 2010. Interaction between human prion protein and amyloid-beta (Abeta) oligomers: role OF N-terminal residues. *J Biol Chem*, 285**,** 26377-83.

CHIANINI, F., FERNANDEZ-BORGES, N., VIDAL, E., GIBBARD, L., PINTADO, B., DE CASTRO, J., PRIOLA, S. A., HAMILTON, S., EATON, S. L., FINLAYSON, J., PANG, Y., STEELE, P., REID, H. W., DAGLEISH, M. P. & CASTILLA, J. 2012. Rabbits are not resistant to prion infection. *Proc Natl Acad Sci U S A*, 109**,** 5080-5.

COLBY, D. W. & PRUSINER, S. B. 2011. Prions. *Cold Spring Harb Perspect Biol,* 3**,** a006833.

CONNOLLY, J. B., ROBERTS, I. J., ARMSTRONG, J. D., KAISER, K., FORTE, M., TULLY, T. & O'KANE, C. J. 1996. Associative learning disrupted by impaired Gs signaling in Drosophila mushroom bodies. *Science,* 274**,** 2104-7.

DAVIS, R. L. 2005. Olfactory memory formation in Drosophila: from molecular to systems neuroscience. *Annu Rev Neurosci,* 28**,** 275-302.

ERANA, H., FERNANDEZ-BORGES, N., ELEZGARAI, S. R., HARRATHI, C., CHARCO, J. M., CHIANINI, F., DAGLEISH, M. P., ORTEGA, G., MILLET, O. & CASTILLA, J. 2017. In Vitro Approach To Identify Key Amino Acids in Low Susceptibility of Rabbit Prion Protein to Misfolding. *J Virol,* 91.

ESPINOSA, J. C., MARIN-MORENO, A., AGUILAR-CALVO, P., BENESTAD, S. L., ANDREOLETTI, O. & TORRES, J. M. 2020. Porcine Prion Protein as a Paradigm of Limited Susceptibility to Prion Strain Propagation. *J Infect Dis*.

FERNANDEZ-BORGES, N., PARRA, B., VIDAL, E., ERANA, H., SANCHEZ-MARTIN, M. A., DE CASTRO, J., ELEZGARAI, S. R., PUMAROLA, M., MAYORAL, T. & CASTILLA, J. 2017. Unraveling the key to the resistance of canids to prion diseases. *PLoS Pathog,* 13**,** e1006716.

FERNANDEZ-FUNEZ, P., CASAS-TINTO, S., ZHANG, Y., GOMEZ-VELAZQUEZ, M., MORALES-GARZA, M. A., CEPEDA-NIETO, A. C., CASTILLA, J., SOTO, C. & RINCON-LIMAS, D. E. 2009. In vivo generation of neurotoxic prion protein: role for hsp70 in accumulation of misfolded isoforms. *PLoS Genet,* 5**,** e1000507.

FERNANDEZ-FUNEZ, P., NINO-ROSALES, M. L., DE GOUYON, B., SHE, W. C., LUCHAK, J. M., MARTINEZ, P., TURIEGANO, E., BENITO, J., CAPOVILLA, M., SKINNER, P. J., MCCALL, A., CANAL, I., ORR, H. T., ZOGHBI, H. Y. & BOTAS, J. 2000. Identification of genes that modify ataxin-1-induced neurodegeneration. *Nature,* 408**,** 101-6.

FERNANDEZ-FUNEZ, P., SANCHEZ-GARCIA, J. & RINCON-LIMAS, D. E. 2017. Drosophila models of prionopathies: insight into prion protein function, transmission, and neurotoxicity. *Curr Opin Genet Dev,* 44**,** 141-148.

FERNANDEZ-FUNEZ, P., ZHANG, Y., CASAS-TINTO, S., XIAO, X., ZOU, W. Q. & RINCON-LIMAS, D. E. 2010. Sequence-dependent prion protein misfolding and neurotoxicity. *J Biol Chem,* 285**,** 36897-36908.

GAVIN, B. A., DOLPH, M. J., DELEAULT, N. R., GEOGHEGAN, J. C., KHURANA, V., FEANY, M. B., DOLPH, P. J. & SUPATTAPONE, S. 2006. Accelerated accumulation of misfolded prion protein and spongiform degeneration in a Drosophila model of Gerstmann-Straussler-Scheinker syndrome. *J Neurosci,* 26**,** 12408-14.

GIBBS, C. J., JR. & GAJDUSEK, D. C. 1973. Experimental subacute spongiform virus encephalopathies in primates and other laboratory animals. *Science,* 182**,** 67-68.

GIMBEL, D. A., NYGAARD, H. B., COFFEY, E. E., GUNTHER, E. C., LAUREN, J., GIMBEL, Z. A. & STRITTMATTER, S. M. 2010. Memory impairment in transgenic Alzheimer mice requires cellular prion protein. *J Neurosci,* 30**,** 6367-74.

GUNTHER, E. C. & STRITTMATTER, S. M. 2010. Beta-amyloid oligomers and cellular prion protein in Alzheimer's disease. *J Mol Med,* 88**,** 331-8.

HETZ, C. 2012. The unfolded protein response: controlling cell fate decisions under ER stress and beyond. *Nat Rev Mol Cell Biol,* 13**,** 89-102.

HETZ, C., CASTILLA, J. & SOTO, C. 2007. Perturbation of endoplasmic reticulum homeostasis facilitates prion replication. *J Biol Chem,* 282**,** 12725-33.

HETZ, C., RUSSELAKIS-CARNEIRO, M., MAUNDRELL, K., CASTILLA, J. & SOTO, C. 2003. Caspase-12 and endoplasmic reticulum stress mediate neurotoxicity of pathological prion protein. *Embo J,* 22**,** 5435-45.

HETZ, C., RUSSELAKIS-CARNEIRO, M., WALCHLI, S., CARBONI, S., VIAL-KNECHT, E., MAUNDRELL, K., CASTILLA, J. & SOTO, C. 2005. The disulfide isomerase Grp58 is a protective factor against prion neurotoxicity. *J Neurosci,* 25**,** 2793-802.

HUGHES, D. & MALLUCCI, G. R. 2019. The unfolded protein response in neurodegenerative disorders - therapeutic modulation of the PERK pathway. *FEBS J,* 286**,** 342-355.

JAMES, T. L., LIU, H., ULYANOV, N. B., FARR-JONES, S., ZHANG, H., DONNE, D. G., KANEKO, K., GROTH, D., MEHLHORN, I., PRUSINER, S. B. & COHEN, F. E. 1997. Solution structure of a 142-residue recombinant prion protein corresponding to the infectious fragment of the scrapie isoform. *Proc Natl Acad Sci U S A,* 94**,** 10086-91.

KANEKO, K., VEY, M., SCOTT, M., PILKUHN, S., COHEN, F. E. & PRUSINER, S. B. 1997. COOH-terminal sequence of the cellular prion protein directs subcellular trafficking and controls conversion into the scrapie isoform. *Proc Natl Acad Sci U S A,* 94**,** 2333-8.

KANG, K., RYOO, H. D., PARK, J. E., YOON, J. H. & KANG, M. J. 2015. A Drosophila Reporter for the Translational Activation of ATF4 Marks Stressed Cells during Development. *PLoS One,* 10**,** e0126795.

KANG, M. J., VASUDEVAN, D., KANG, K., KIM, K., PARK, J. E., ZHANG, N., ZENG, X., NEUBERT, T. A., MARR, M. T., 2ND & RYOO, H. D. 2017. 4E-BP is a target of the GCN2-ATF4 pathway during Drosophila development and aging. *J Cell Biol,* 216**,** 115-129.

KESSELS, H. W., NGUYEN, L. N., NABAVI, S. & MALINOW, R. 2010. The prion protein as a receptor for amyloid-beta. *Nature,* 466**,** E3-4; discussion E4-5.

KHAN, M. Q., SWEETING, B., MULLIGAN, V. K., ARSLAN, P. E., CASHMAN, N. R., PAI, E. F. & CHAKRABARTTY, A. 2010. Prion disease susceptibility is affected by beta-structure folding propensity and local side-chain interactions in PrP. *Proc Natl Acad Sci U S A,* 107**,** 19808-13.

KIM, K., PARK, J. E., YEOM, J., PARK, N., TRAN, T. T. & KANG, M. J. 2020. Tissue-specific roles of GCN2 in aging and autosomal dominant retinitis pigmentosa. *Biochem Biophys Res Commun,* 533**,** 1054-1060.

KIRKWOOD, J. K. & CUNNINGHAM, A. A. 1994. Epidemiological observations on spongiform encephalopathies in captive wild animals in the British Isles. *Vet Rec,* 135**,** 296-303.

KOBAYASHI, A., TERUYA, K., MATSUURA, Y., SHIRAI, T., NAKAMURA, Y., YAMADA, M., MIZUSAWA, H., MOHRI, S. & KITAMOTO, T. 2015. The influence of PRNP polymorphisms on human prion disease susceptibility: an update. *Acta Neuropathol,* 130**,** 159-70.

LAUREN, J., GIMBEL, D. A., NYGAARD, H. B., GILBERT, J. W. & STRITTMATTER, S. M. 2009. Cellular prion protein mediates impairment of synaptic plasticity by amyloid-beta oligomers. *Nature,* 457**,** 1128-32.

LE BOURG, E. & LINTS, F. A. 1992. Hypergravity and aging in Drosophila melanogaster. 4. Climbing activity. *Gerontology,* 38**,** 59-64.

LIN, D. M. & GOODMAN, C. S. 1994. Ectopic and increased expression of Fasciclin II alters motoneuron growth cone guidance. *Neuron,* 13**,** 507-23.

LYSEK, D. A., SCHORN, C., NIVON, L. G., ESTEVE-MOYA, V., CHRISTEN, B., CALZOLAI, L., VON SCHROETTER, C., FIORITO, F., HERRMANN, T., GUNTERT, P. & WUTHRICH, K. 2005. Prion protein NMR structures of cats, dogs, pigs, and sheep. *Proc Natl Acad Sci U S A,* 102**,** 640-5.

MALZER, E., DALY, M. L., MOLONEY, A., SENDALL, T. J., THOMAS, S. E., RYDER, E., RYOO, H. D., CROWTHER, D. C., LOMAS, D. A. & MARCINIAK, S. J. 2010. Impaired tissue growth is mediated by checkpoint kinase 1 (CHK1) in the integrated stress response. *J Cell Sci,* 123**,** 2892-900.

MALZER, E., DOMINICUS, C. S., CHAMBERS, J. E., DICKENS, J. A., MOOKERJEE, S. & MARCINIAK, S. J. 2018. The integrated stress response regulates BMP signalling through effects on translation. *BMC Biol,* 16**,** 34.

MALZER, E., SZAJEWSKA-SKUTA, M., DALTON, L. E., THOMAS, S. E., HU, N., SKAER, H., LOMAS, D. A., CROWTHER, D. C. & MARCINIAK, S. J. 2013. Coordinate regulation of eIF2alpha phosphorylation by PPP1R15 and GCN2 is required during Drosophila development. *J Cell Sci,* 126**,** 1406-15.

MATHIASON, C. K. 2017. Scrapie, CWD, and Transmissible Mink Encephalopathy. *Prog Mol Biol Transl Sci,* 150**,** 267-292.

MOORE, B. D., MARTIN, J., DE MENA, L., SANCHEZ, J., CRUZ, P. E., CEBALLOS-DIAZ, C., LADD, T. B., RAN, Y., LEVITES, Y., KUKAR, T. L., KURIAN, J. J., MCKENNA, R., KOO, E. H., BORCHELT, D. R., JANUS, C., RINCON-LIMAS, D., FERNANDEZ-FUNEZ, P. & GOLDE, T. E. 2018. Short Abeta peptides attenuate Abeta42 toxicity in vivo. *J Exp Med,* 215**,** 283-301.

MORENO, J. A., RADFORD, H., PERETTI, D., STEINERT, J. R., VERITY, N., MARTIN, M. G., HALLIDAY, M., MORGAN, J., DINSDALE, D., ORTORI, C. A., BARRETT, D. A., TSAYTLER, P., BERTOLOTTI, A., WILLIS, A. E., BUSHELL, M. & MALLUCCI, G. R. 2012. Sustained translational repression by eIF2alpha-P mediates prion neurodegeneration. *Nature,* 485**,** 507-11.

MYERS, R., CEMBRAN, A. & FERNANDEZ-FUNEZ, P. 2020. Insight From Animals Resistant to Prion Diseases: Deciphering the Genotype – Morphotype – Phenotype Code for the Prion Protein. *Front. Cell. Neurosci.,* 14.

OTERO, A., HEDMAN, C., FERNANDEZ-BORGES, N., ERANA, H., MARIN, B., MONZON, M., SANCHEZ-MARTIN, M. A., NONNO, R., BADIOLA, J. J., BOLEA, R. & CASTILLA, J. 2019. A Single Amino Acid Substitution, Found in Mammals with Low Susceptibility to Prion Diseases, Delays Propagation of Two Prion Strains in Highly Susceptible Transgenic Mouse Models. *Mol Neurobiol,* 56**,** 6501-6511.

PEREZ, D. R., DAMBERGER, F. F. & WUTHRICH, K. 2010. Horse prion protein NMR structure and comparisons with related variants of the mouse prion protein. *J Mol Biol,* 400**,** 121-8.

PFEIFFER, B. D., NGO, T. T., HIBBARD, K. L., MURPHY, C., JENETT, A., TRUMAN, J. W. & RUBIN, G. M. 2010. Refinement of tools for targeted gene expression in Drosophila. *Genetics,* 186**,** 735-55.

RIEK, R., HORNEMANN, S., WIDER, G., BILLETER, M., GLOCKSHUBER, R. & WUTHRICH, K. 1996. NMR structure of the mouse prion protein domain PrP(121-321). *Nature,* 382**,** 180-2.

ROMAN, G., ENDO, K., ZONG, L. & DAVIS, R. L. 2001. P[Switch], a system for spatial and temporal control of gene expression in Drosophila melanogaster. *Proc Natl Acad Sci U S A,* 98**,** 12602-7.

RUBIN, G. M. & SPRADLING, A. C. 1982. Genetic transformation of Drosophila with transposable element vectors. *Science,* 218**,** 348-53.

RYOO, H. D., DOMINGOS, P. M., KANG, M. J. & STELLER, H. 2007. Unfolded protein response in a Drosophila model for retinal degeneration. *Embo J,* 26**,** 242-52.

SANCHEZ-GARCIA, J., CASAS-TINTO, S., RINCON-LIMAS, D. & FERNANDEZ FUNEZ, P. 2013. Protein Misfolding in Drosophila Models of Prionopathies. *Protein purification and analysis I: methods and applications.* iConcept Press.

SANCHEZ-GARCIA, J. & FERNANDEZ-FUNEZ, P. 2018. D159 and S167 are protective residues in the prion protein from dog and horse, two prion-resistant animals. *Neurobiol Dis,* 119**,** 1-12.

SANDBERG, M. K., AL-DOUJAILY, H., SHARPS, B., CLARKE, A. R. & COLLINGE, J. 2011. Prion propagation and toxicity in vivo occur in two distinct mechanistic phases. *Nature,* 470**,** 540-2.

SANDBERG, M. K., AL-DOUJAILY, H., SHARPS, B., DE OLIVEIRA, M. W., SCHMIDT, C., RICHARD-LONDT, A., LYALL, S., LINEHAN, J. M., BRANDNER, S., WADSWORTH, J. D., CLARKE, A. R. & COLLINGE, J. 2014. Prion neuropathology follows the accumulation of alternate prion protein isoforms after infective titre has peaked. *Nat Commun,* 5**,** 4347.

SCHECKEL, C. & AGUZZI, A. 2018. Prions, prionoids and protein misfolding disorders. *Nat Rev Genet*.

SIGURDSON, C. J., BARTZ, J. C. & GLATZEL, M. 2019. Cellular and Molecular Mechanisms of Prion Disease. *Annu Rev Pathol,* 14**,** 497-516.

SIGURDSON, C. J. & MILLER, M. W. 2003. Other animal prion diseases. *Br Med Bull,* 66**,** 199-212.

SOKAL, R. R. & ROHLF, F. J. 2012. *Biometry : the principles and practice of statistics in biological research,* New York, W.H. Freeman.

STEELE, A. D., LINDQUIST, S. & AGUZZI, A. 2007. The prion protein knockout mouse: a phenotype under challenge. *Prion,* 1**,** 83-93.

TANAKA, N. K., TANIMOTO, H. & ITO, K. 2008. Neuronal assemblies of the Drosophila mushroom body. *J Comp Neurol,* 508**,** 711-55.

TAYLOR, R. C. & DILLIN, A. 2013. XBP-1 is a cell-nonautonomous regulator of stress resistance and longevity. *Cell,* 153**,** 1435-47.

TELLING, G. C., SCOTT, M., MASTRIANNI, J., GABIZON, R., TORCHIA, M., COHEN, F. E., DEARMOND, S. J. & PRUSINER, S. B. 1995. Prion propagation in mice expressing human and chimeric PrP transgenes implicates the interaction of cellular PrP with another protein. *Cell,* 83**,** 79-90.

THACKRAY, A. M., DI, Y., ZHANG, C., WOLF, H., PRADL, L., VORBERG, I., ANDREOLETTI, O. & BUJDOSO, R. 2014. Prion-induced and spontaneous formation of transmissible toxicity in PrP transgenic Drosophila. *Biochem J,* 463**,** 31-40.

THACKRAY, A. M., MUHAMMAD, F., ZHANG, C., DENYER, M., SPIROPOULOS, J., CROWTHER, D. C. & BUJDOSO, R. 2012a. Prion-induced toxicity in PrP transgenic Drosophila. *Exp Mol Pathol,* 92**,** 194-201.

THACKRAY, A. M., MUHAMMAD, F., ZHANG, C., DI, Y., JAHN, T. R., LANDGRAF, M., CROWTHER, D. C., EVERS, J. F. & BUJDOSO, R. 2012b. Ovine PrP transgenic Drosophila show reduced locomotor activity and decreased survival. *Biochem J,* 444**,** 487-95.

VASUDEVAN, D., CLARK, N. K., SAM, J., COTHAM, V. C., UEBERHEIDE, B., MARR, M. T., 2ND & RYOO, H. D. 2017. The GCN2-ATF4 Signaling Pathway Induces 4E-BP to Bias Translation and Boost Antimicrobial Peptide Synthesis in Response to Bacterial Infection. *Cell Rep,* 21**,** 2039-2047.

VIDAL, E., FERNANDEZ-BORGES, N., ERANA, H., PARRA, B., PINTADO, B., SANCHEZ-MARTIN, M. A., CHARCO, J. M., ORDONEZ, M., PEREZ-CASTRO, M. A., PUMAROLA, M., MATHIASON, C. K., MAYORAL, T. & CASTILLA, J. 2020. Dogs are resistant to prion infection, due to the presence of aspartic or glutamic acid at position 163 of their prion protein. *FASEB J,* 34**,** 3969-3982.

VILETTE, D., ANDREOLETTI, O., ARCHER, F., MADELAINE, M. F., VILOTTE, J. L., LEHMANN, S. & LAUDE, H. 2001. Ex vivo propagation of infectious sheep scrapie agent in heterologous epithelial cells expressing ovine prion protein. *Proc Natl Acad Sci U S A,* 98**,** 4055-9.

VORBERG, I., GROSCHUP, M. H., PFAFF, E. & PRIOLA, S. A. 2003. Multiple amino acid residues within the rabbit prion protein inhibit formation of its abnormal isoform. *J Virol,* 77**,** 2003-9.

ZAHN, R., LIU, A., LUHRS, T., RIEK, R., VON SCHROETTER, C., LOPEZ GARCIA, F., BILLETER, M., CALZOLAI, L., WIDER, G. & WUTHRICH, K. 2000. NMR solution structure of the human prion protein. *Proc Natl Acad Sci U S A,* 97**,** 145-50.

ZHANG, Y., ZHAO, Y., ZHANG, L., YU, W., WANG, Y. & CHANG, W. 2019. Cellular Prion Protein as a Receptor of Toxic Amyloid-beta42 Oligomers Is Important for Alzheimer's Disease. *Front Cell Neurosci,* 13**,** 339.

ZLOTNIK, I. & RENNIE, J. C. 1963. Further observations on the experimental transmission of scrapie from sheep and goats to laboratory mice. *J Comp Pathol,* 73**,** 150-62.

ZLOTNIK, I. & RENNIE, J. C. 1965. Experimental Transmission of Mouse Passaged Scrapie to Goats, Sheep, Rats and Hamsters. *J Comp Pathol,* 75**,** 147-57.

ZOU, W. Q., XIAO, X., YUAN, J., PUOTI, G., FUJIOKA, H., WANG, X., RICHARDSON, S., ZHOU, X., ZOU, R., LI, S., ZHU, X., MCGEER, P. L., MCGEEHAN, J., KNEALE, G., RINCON-LIMAS, D. E., FERNANDEZ-FUNEZ, P., LEE, H. G., SMITH, M. A., PETERSEN, R. B. & GUO, J. P. 2011. Amyloid-beta42 interacts mainly with insoluble prion protein in the Alzheimer brain. *J Biol Chem,* 286**,** 15095-105.

Figures

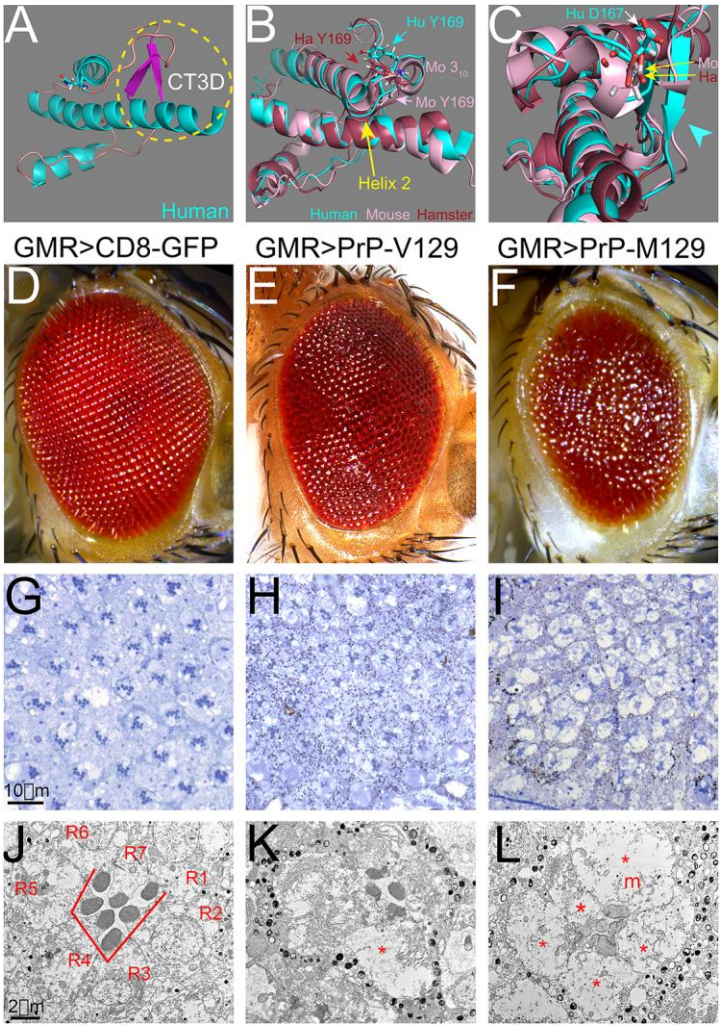

Figure 1. New eye phenotypes of random human PrP lines. A-C, 3D visualization of the PrP globular domain. **A**, Human PrP and the CT3D domain (circle). **B and C**, 3D alignment of human (cyan), mouse (pink) and hamster (brown) globular domains show high conservation. Mouse has a 3_{10} turn in the loop and a longer helix 2 (C, arrow). The position of D167 and Y169 are indicated (B and C). The β-sheet has different length (C, arrowhead). **D-L**, Eyes from flies expressing GFP (*GMR-Gal4* / *UAS-mCD8-GFP*) (D, G, and J), human PrP-V129 (*GMR-Gal4 / UAS-R-human PrP-V129*) (E, H and K), or human PrP-M129 (*GMR-Gal4 / UAS-R-human PrP-M129*) (F, I and L) from random insertions at 27˚C. **D-F**,

Micrographs of fresh eyes. Control flies and flies expressing *mCD8-GFP* exhibit highly organized eyes (D). Flies expressing human PrP-V129 or M129 display disorganized eyes. **G-I,** Semithin sections of the retina. G, Expression of GFP preserves the lattice and photoreceptors. H, Expression of PrP-V129 results in disorganized ommatidia and loss of photoreceptors. I, Expression of PrP-M129 results in vacuolated retina with loss of photoreceptors. **J-L**, Transmission electron micrographs of single ommatidia. J, Expression of GFP preserves seven photoreceptors (R1-R7) and rhabdomeres. K, Expression of PrP-V129 results in partial vacuolation of photoreceptors (*), abnormal rhabdomeres, and excess of ER (arrowheads). L, Expression of PrP-M129 results in vacuolated photoreceptors (*) and mitochondria (m), and hypochromic rhabdomeres.

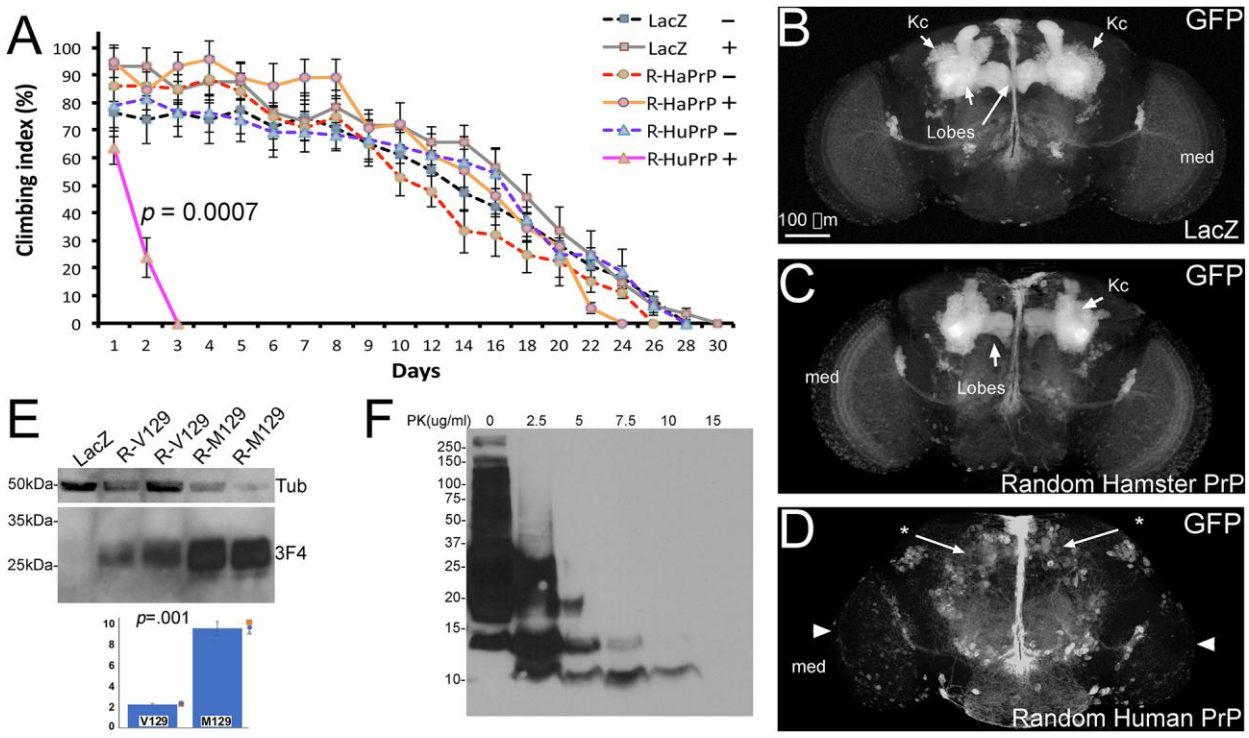

Figure 2. New phenotypes induced by human PrP in *Drosophila*. A, Random insertions of human PrP induce aggressive locomotor dysfunction**.** Conditional pan-neural expression of LacZ (squares, *Elav-GS; UAS-LacZ*), hamster PrP (circles, *Elav-GS; UAS-R-HaPrP*), and human PrP (triangles, *Elav-GS; UAS-R-HuPrP-V129*). Expression was activated at day 1 (+, continuous line) or not activated (-, broken line) (n=2). Only flies expressing human PrP exhibit locomotor dysfunction. **B-D,** Expression of human PrP in the mushroom bodies. B, Expression of LacZ (*OK107-Gal4 / UAS-mCD8-GFP / UAS-LacZ*) reveals large mushroom body (MB) clusters in 1-day-old flies, including Kenyon cell clusters (Kc) and axonal lobes. C, Expression of hamster PrP (*OK107-Gal4 / UAS-mCD8-GFP / UAS-R-HaPrP*) has no effect on the MB. D, Expression of human PrP-V129 (*OK107-Gal4 / UAS-mCD8-GFP / UAS-R-HuPrP-V129*) eliminates the mushroom bodies and results in a smaller medulla (med, arrowhead). **E,** Fly homogenates expressing LacZ (lane 1), human PrP-V129 (lanes 2 and 3), or human PrP-M129 (lanes 4 and 5) in the eye from random insertions at 27˚C (same genotypes as in figure 1). V129 and M129 display similar electrophoretic mobility (3F4 anti-PrP antibody), but M129 accumulates at over 4 times higher levels as

indicated by bar graph (n=3). **F,** Homogenates from 10-day-old heads expressing human PrP in the eye subjected to a mild PK gradient. The 10 μg/ml treatment degraded most PrP except for a 10 kDa fragment. The 15 μm/ml digestion has no detectable PrP.

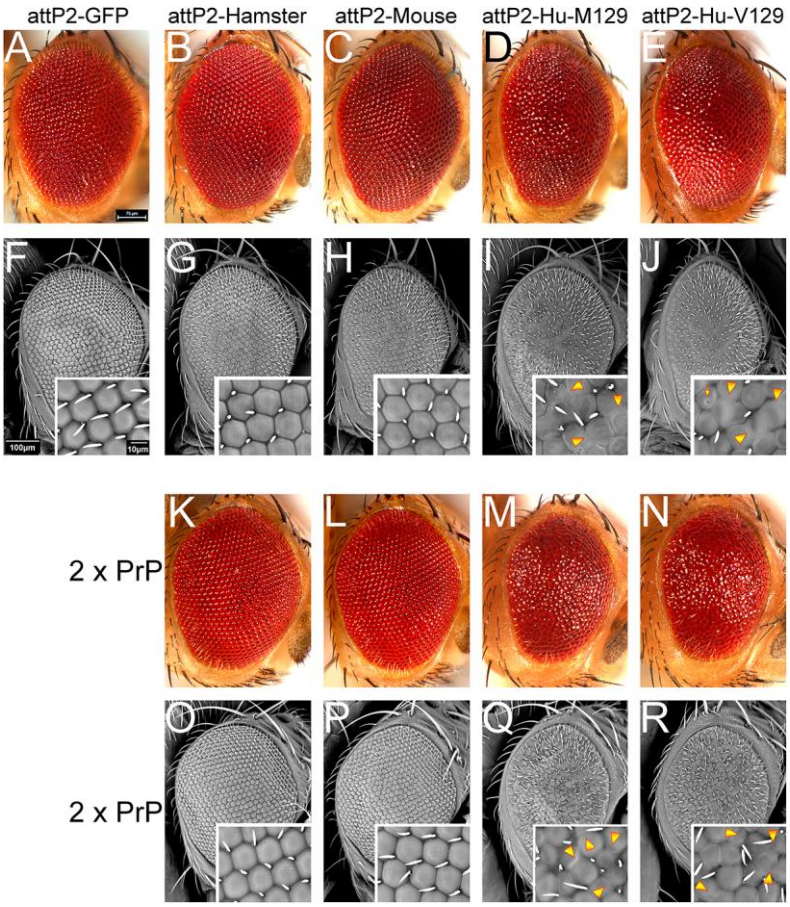

Figure 3. Human PrP-attP2 constructs are more toxic than rodent PrP-attP2. Fresh eyes and scanning electron micrographs of eyes expressing the attP2-PrP constructs. **A-J**, one copy of PrP constructs, **K-R**, two copies. **A and F**, Control eyes from flies expressing mCD8-GFP-attP2 (*GMR-Gal4 / UAS-mCD8-GFP-attP2*) display a highly organized lattice. Flies expressing PrP from hamster (**B and G**) (*GMR-Gal4 / UAS-hamster PrP-attP2*) or mouse (**C and H**) (*GMR-Gal4 / UAS-mouse PrP-attP2*) show normal eyes. **D, E, I and J**, Flies expressing human PrP (*GMR-Gal4 / UAS-human PrP-M129-attP2* or *GMR-Gal4 / UAS-human PrP-V129-attP2*) display mildly disorganized eyes. **K-R**, Flies expressing two PrP copies (2X) (*GMR-Gal4 / +; UAS-PrP-attP2 / UAS-PrP-attP2*). Flies expressing two copies of hamster (**K and O**), or mouse (**L and P**) PrP display well organized eyes. **M, N, Q and R**, Flies expressing human PrP-M129 or PrP-V129 display smaller and glassy eyes.

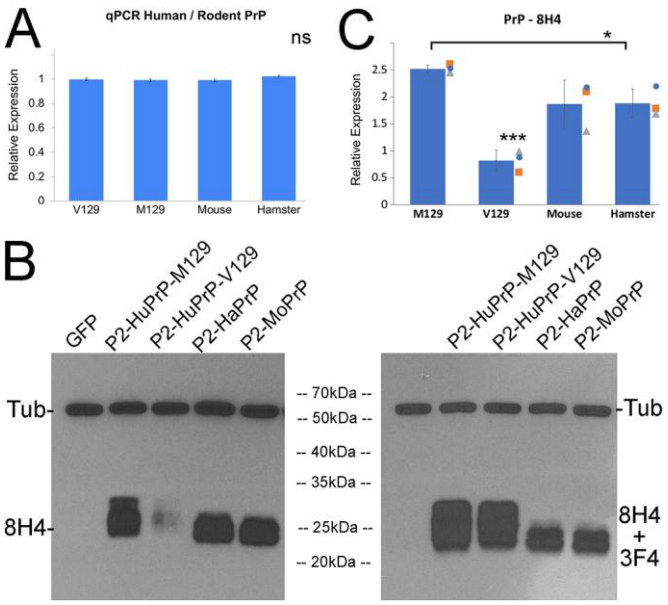

Figure 4. Human and rodent PrP undergo different biogenesis. A-C, Expression of attP-based constructs in the eye (same genotypes as in figure 3). **A**, Levels of PrP mRNA by qPCR are identical for all PrP construct (2 independent experiments). **B**, Western blot. Left: detection of PrP with 8H4 anti-PrP and anti-Tubulin from fly heads expressing the indicated construct in the eyes. The electrophoretic pattern of human M129 is different to rodent PrP. V129 is weak with 8H4. Right: same membrane serially incubated with 8H4 and 3F4 antibodies showing normal levels of human V129. C, Quantification of PrP signal with the 8H4 antibody (n=3). * $p< 0.05$; *** $p < 0.001$.

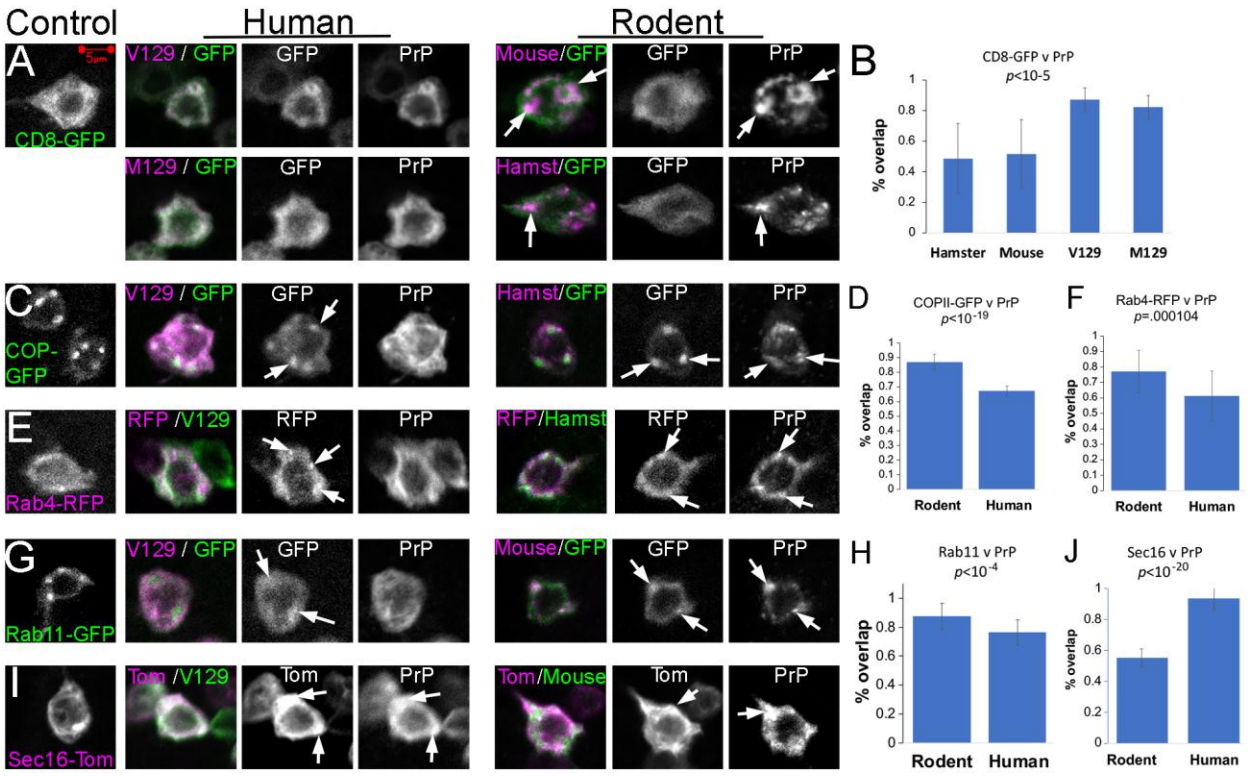

Figure 5. Subcellular distribution of rodent and human PrP. D-F, Distribution of human PrP in interneurons of the larval ventral ganglion (*OK107-Gal4 / UAS-attP2-PrP / UAS-GFP-X*). **A**, Co-expression of *UAS-mCD8-GFP* and *UAS-LacZ* (control), human PrP (*UAS-attP2-HuPrP-V129 or UAS-attP2-HuPrP-M129*) or rodent PrP (*UAS-attP2-hamster PrP or UAS-attP2-mouse PrP*). Human PrP shows diffuse expression and rodent PrP has punctate distribution. **B**, Fraction of mCD8-GFP and PrP overlap. **C**, Co-expression of *UAS-COPII-GFP* and *UAS-LacZ* (control), human PrP (*UAS-attP2-HuPrP-V129*) or rodent PrP (*UAS-attP2-hamster PrP*). **D**, Fraction of COPII-GFP and PrP overlap. **E**, Co-expression of *UAS-Rab4-RFP* and LacZ (control), human PrP (*UAS-attP2-HuPrP-V129*) or rodent PrP (*UAS-attP2-hamster PrP*). **F**, Fraction of Rab4-RFP and PrP overlap. **G**, Co-expression of *UAS-Rab11-GFP* and LacZ (control), human PrP (*UAS-attP2-HuPrP-V129*) or rodent PrP (*UAS-attP2-mouse PrP*). **H**, Fraction of Rab11-GFP and PrP overlap. **I**, Co-expression of *UAS- Sec16-Tomato* and LacZ (control), human PrP (*UAS-attP2-HuPrP-V129*) or rodent PrP (*UAS-attP2-mouse PrP*). **H**, Fraction of *Sec16-Tomato* and PrP overlap. All images collected at the same magnification (scale bar in panel A same for all panels). Data was created from 12-15 neurons from observations replicated in > 6 brains.

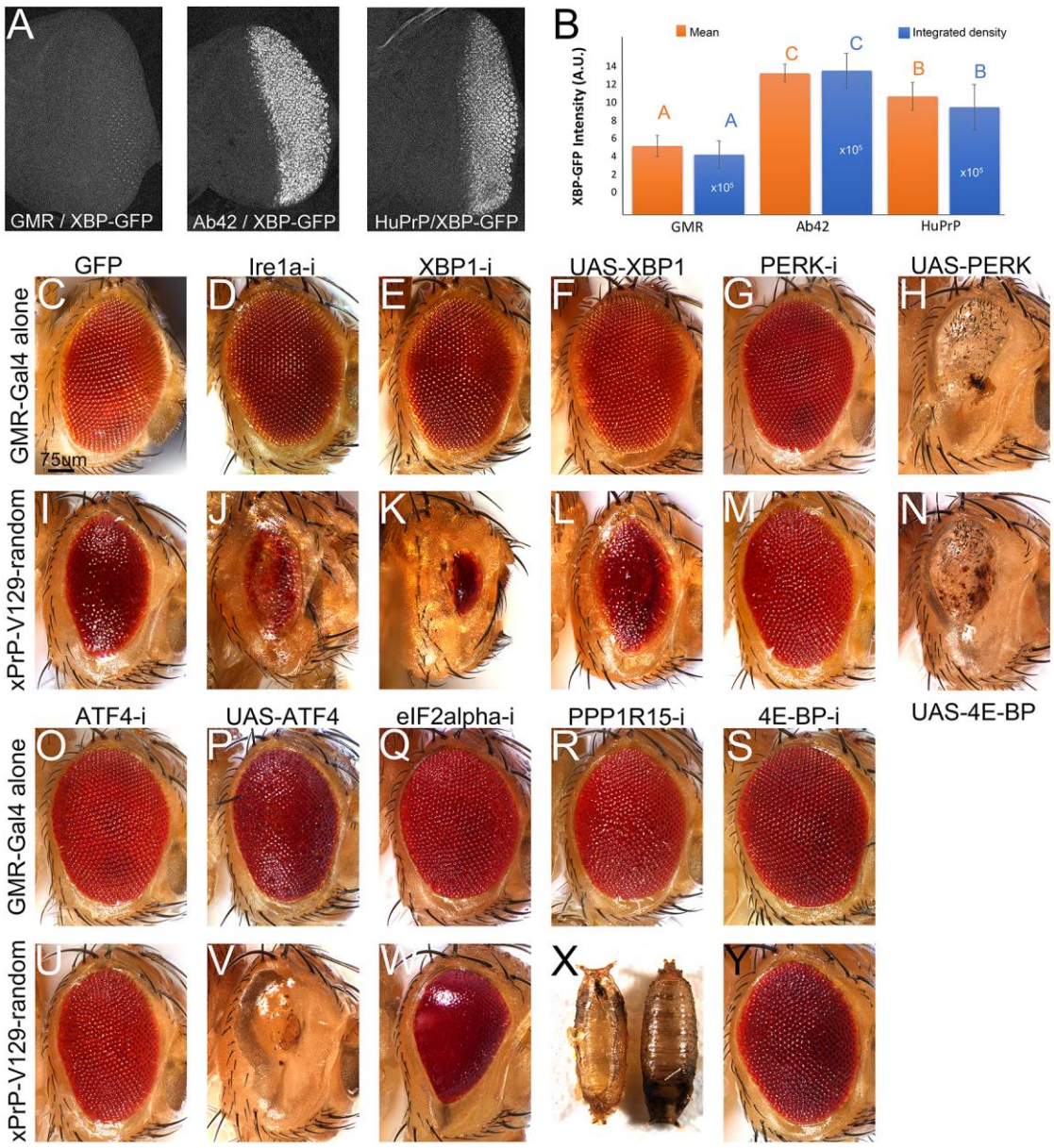

Figure 6. Silencing PERK and ATF4 suppresses human PrP toxicity. A and B, Human PrP activates the XBP-GFP sensor (*GMR-Gal4 / UAS-XBP-GFP*). Both human PrP (*UAS-R-Human PrP-V129*) and Aβ42 (*UAS-R-Aβ42*) activate XBP-GFP above the endogenous levels, but Aβ42 is stronger. **B**, Mean signal (orange) and integrated intensity (blue) are analyzed independently. Scale for the integrated density is x10^5. All differences for are statistically significant as indicated by non-overlapping letters from ANOVA. **C-Z**, Micrographs of fresh eyes expressing UPR alleles alone or in combination with human

PrP in the eye at 27˚C. **C and I**, Control flies expressing mCD8-GFP (C, *GMR-Gal4 / UAS-mCD8-GFP-attP2*) or co-expressing PrP (I, *GMR-Gal4 / UAS-mCD8-GFP-attP2 / UAS-R-human PrP-V129*). **D-F,** Flies carrying Ire1α branch alleles (D, *GMR-Gal4 / UAS-Ire1α-RNAi*), XBP1-RNAi (E, *GMR-Gal4 / UAS-XBP1-RNAi*) or XBP1 (F, *GMR-Gal4 / UAS-XBP1*) alone exhibit normal eyes. **J and K,** Flies co-expressing PrP and Ire1α-RNAi (J, *GMR-Gal4 / UAS-Ire1α-RNAi / UAS-R-human PrP-V129*) or XBP1-RNAi (K, *GMR-Gal4 / UAS-XBP1-RNAi / UAS-R-human PrP-V129*) exhibit small eyes. **L,** Flies co-expressing PrP and XBP1 (*GMR-Gal4 / UAS-XBP1 / UAS-R-human PrP-V129*) show no change. **G and O**, Flies expressing PERK-RNAi (G, *GMR-Gal4 / UAS-PERK-RNAi*) or ATF4-RNAi (O, *GMR-Gal4 / UAS-ATF4-RNAi*) alone exhibit normal eyes. **M and U,** Flies co-expressing PrP and PERK-RNAi (M, *GMR-Gal4 / UAS-PEK-RNAi / UAS-R-human PrP-V129*) or ATF4-RNAi (U, *GMR-Gal4 / UAS-ATF4-RNAi / UAS-R-human PrP-V129*) exhibit large eyes. **H and N,** Flies expressing PERK alone (H, *GMR-Gal4 / UAS-PERK*) or co-expressing PrP (N, *GMR-Gal4 / UAS-PERK / UAS-R-human PrP-V129*) have small eyes. **P,** Flies expressing ATF4 (*GMR-Gal4 / UAS-ATF4*) have mildly disorganized eyes. **V,** Flies co-expressing PrP and ATF4 (*GMR-Gal4 / UAS-ATF4 / UAS-R-human PrP-V129*) show small eyes.. **Q**, Flies expressing eIF2α-RNAi (*GMR-Gal4 / UAS-eIF2α-RNAi*) exhibit mildly disorganized eyes. **W,** Flies co-expressing PrP and eIF2α-RNAi (*GMR-Gal4 / UAS-eIF2α-RNAi / UAS-R-human PrP-V129*) exhibit highly disorganized and mildly depigmented eyes. **R**, Flies expressing PPP1R15-RNAi (*GMR-Gal4 / UAS-PPP1R15-RNAi*) show mildly disorganized eyes. **X,** Flies co-expressing PrP and PPP1R15-RNAi (*GMR-Gal4 / UAS-PPP1R15-RNAi / UAS-R-human PrP-V129*) results in pupal lethality. **S and Y**, Flies expressing 4E-BP-RNAi alone (S, *GMR-Gal4 / UAS-4E-BP-RNAi*) show normal eyes; co-expressing PrP (Y, *GMR-Gal4 / UAS-4E-BP-RNAi / UAS-R-human PrP-V129*) suppresses toxicity. **T and X**, Flies expressing 4E-BP alone (T, *GMR-Gal4 / UAS-4E-BP*) show normal eyes and co-expressing PrP (*GMR-Gal4 / UAS-4E-BP / UAS-R-human PrP-V129*) enhances toxicity. Each observation was independently replicated at least 3 times.

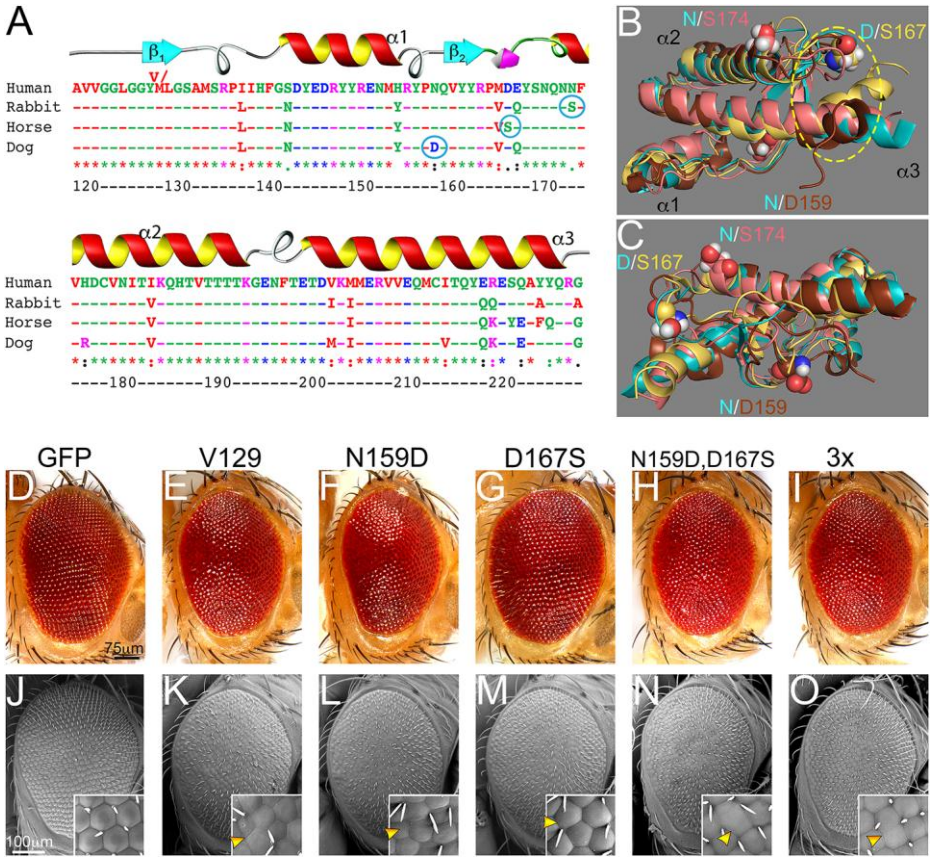

Figure 7. D167S is protective in human PrP. **A**, Sequence alignment of the globular domain of human, dog, horse, and rabbit PrP. Amino acid numbering corresponds to human PrP. Candidate protective residues are circled. **B and C**, 3D alignment of the globular domain of human (cyan), dog (brown), horse (yellow), and rabbit (salmon) PrP. The position of residues 159, 167, and 174 is indicated. **D-O**, Micrographs of fresh eyes and scanning electron microscope from control flies or flies expressing human PrP-attP2. **D and J**, Control flies (*GMR-Gal4 / UAS-mCD8-GFP-attP2*) show large, organized eyes. **E and K**, Flies expressing human PrP-WT (*GMR-Gal4 / UAS-human PrP-V129-attP2*) show disorganized, glassy eyes with ommatidia fusions (arrowhead). **F and L**, Flies expressing PrP-N159D (*GMR-Gal4 / UAS-human PrP-N159D-attP2*) show glassy eyes with abnormal ommatidia (arrowhead). **G and M**, Flies expressing PrP-D167S (*GMR-Gal4 / UAS-human PrP-D167S-attP2*) show improved eye organization (arrowhead). **H, I, N and O**, Flies expressing the 2X mutant PrP (*GMR-Gal4 / UAS-human PrP-N159D-*

D167S-attP2) or the 3X mutant (*GMR-Gal4 / UAS-human PrP-N159D-D167S-N174S-attP2*) show partially rescued eye organization but abnormal ommatidia are visible (arrowheads). Each observation was independently replicated at least 3 times.

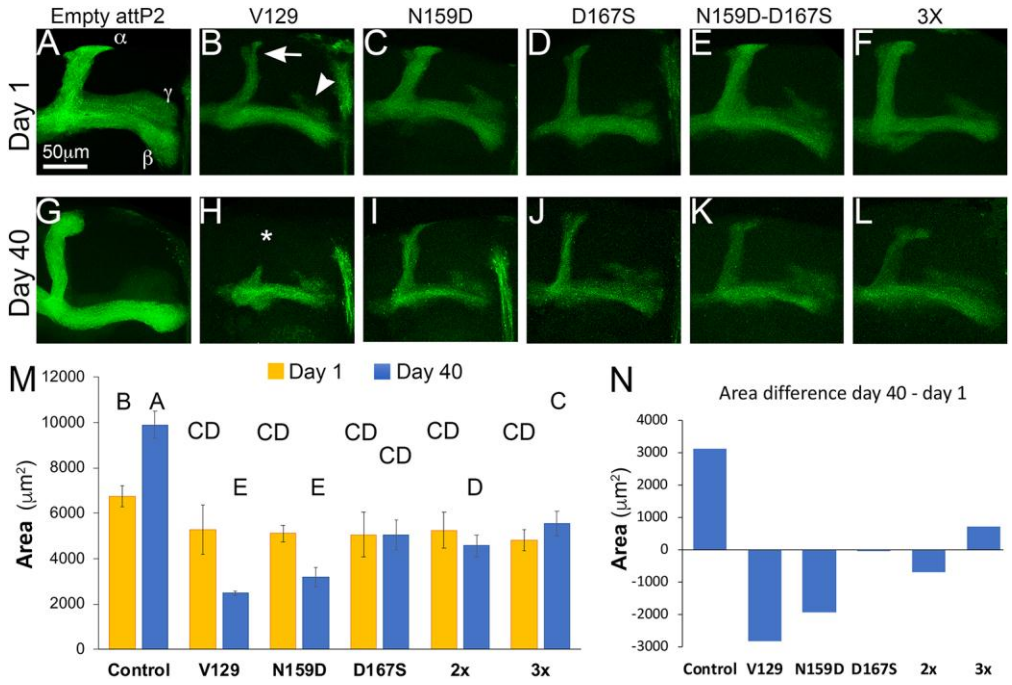

Figure 8. Analysis of protective mutations in brain neurons. A-L, Micrographs of mushroom body axonal projections at days 1 (A-F) or 40 (G-L). **A and G**, 1- and 40-day-old flies carrying an empty attP2 site (*OK107-Gal4 / UAS-mCD8-GFP / attP2*) show robust mushroom body axonal projections. The α, β, and γ lobes are indicated. 40-day-old flies show an increase in projection surface. **B and H**, 1- and 40-day-old flies expressing human PrP-WT (*OK107-Gal4 / UAS-mCD8-GFP / UAS-human PrP-V129-attP2*) show thin projections at day 1 and significant degeneration by day 40 (H, *). **C and I**, 1- and 40-day-old flies expressing PrP-N159D (*OK107-Gal4 /UAS-mCD8-GFP / UAS-human PrP-N159D-attP2*) show small projections at day 1 that continue to degenerate during aging. **D and J**, 1- and 40-day-old flies expressing PrP-D167S (*OK107-Gal4 / UAS-mCD8-GFP / UAS-human PrP-D167S-attP2*) show small projections at day 1 but slower degeneration. **E, F, K and L**, 1- and 40-day-old flies expressing the 2X (*OK107-Gal4 / UAS-mCD8-GFP / UAS-human PrP-N159D-D167S-attP2*) or 3X (*OK107-Gal4 / UAS-mCD8-GFP / UAS-human PrP-N159D-D167S-N174S-attP2*) show small projections at day 1 but slower degeneration. **M**, Quantification of axonal projections. Statistical significance between groups is shown by the connecting letters. Levels not connected by the same letter are significantly different. P-value for

different letter groups is <0.0001 except for B and C (p = 0.0037) and between CD and D (p = 0.021). **N**, Area differential day 40 – day 1 for each condition. Only the control flies and flies expressing the 3X mutant show an expansion of axonal projections over time. Data created from 10-12 brains, analyzed by Two-way ANOVA and adjusted for multiple comparisons.

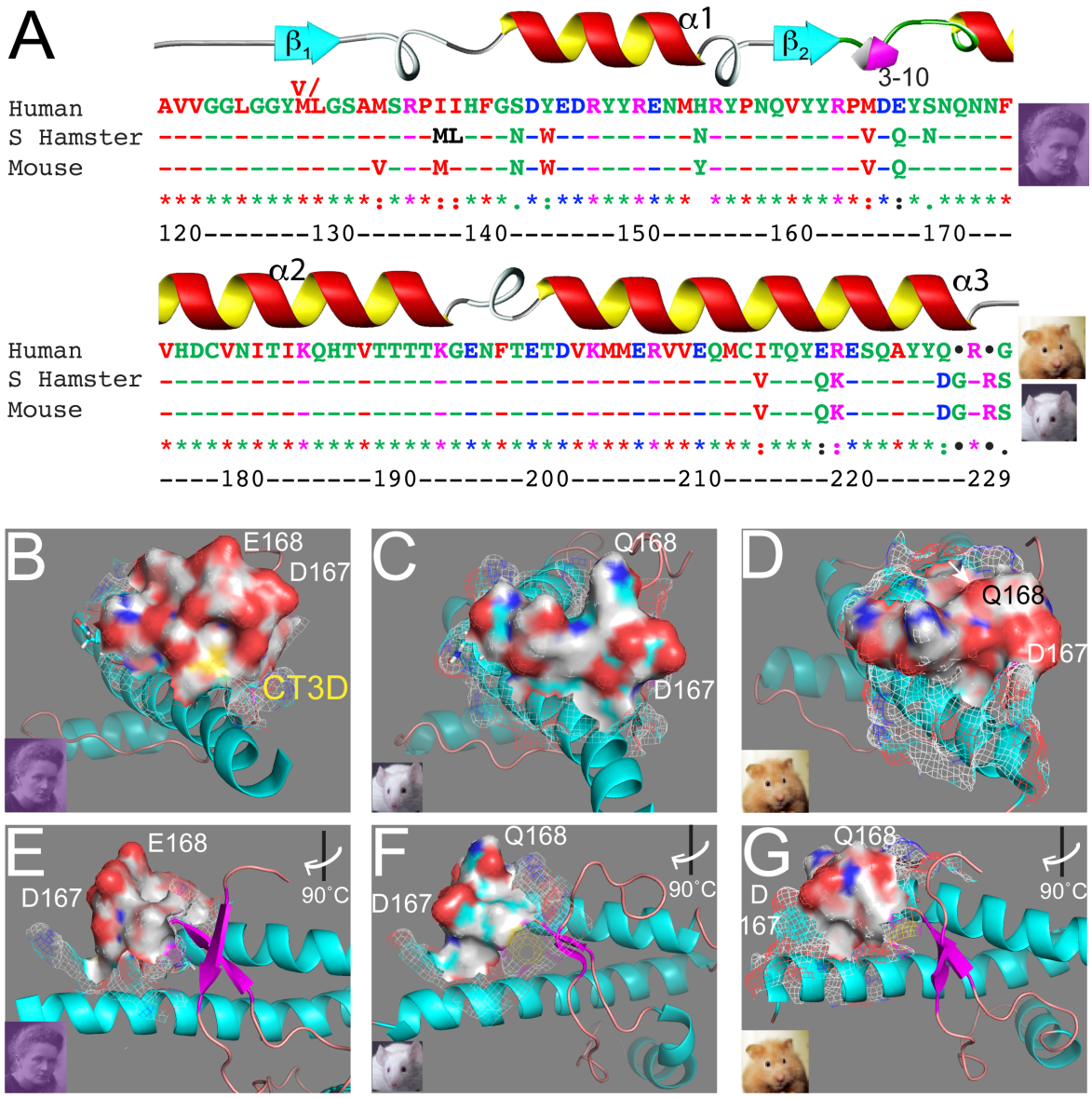

Fig. S1. Sequence / structure differences between human and animal PrP. A, Sequence alignment of the C-terminal globular domain of PrP from human, Syrian hamster, and mouse. Amino acid numbering corresponds to human PrP throughout to avoid confusion. The alignment shows high overall conservation with most variation clustered in the β2-α2 loop and distal helix 3. **B-G**, Surface and Mesh views for the β2-α2 loop, front view (B-D) and side view (E-G). In human PrP, the loop is vertical and tall, with two acidic residues sticking upwards (B and E). In mouse PrP, the loop is not as tall, with D167 shifted to a lower position (C and F). In hamster PrP, the loop is flat and closer to helix 3 (D and G).

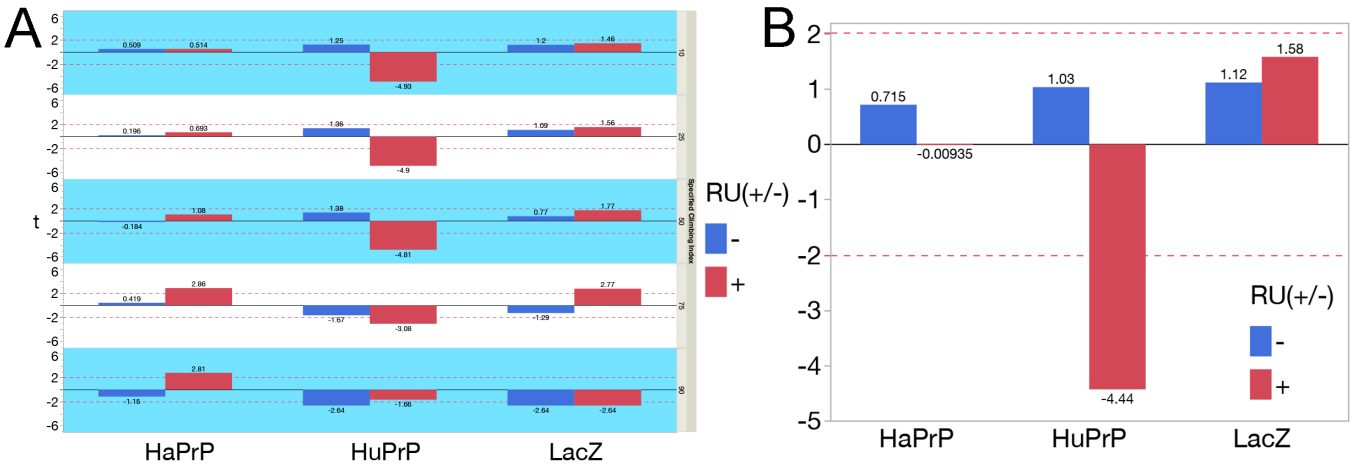

Fig. S2. Statistical analysis of locomotor activity. A, Single-sample t-test analysis of age-dependent climbing index. HuPrP with RU has a significant negative effect on age-specific climbing index. Bars represent t-score. **B**, Area under the curve. Dotted red-line represents the critical value of 2.015 for t-test with 5 degrees of freedom (p<0.05). Single-sample t-test analysis of area under curve for the climbing index. HuPrP with RU has a significant negative effect on area under the climbing index curve. Bars represent t-score. Dotted red-line represents the critical value of 2.015 for t-test with 5 degrees of freedom

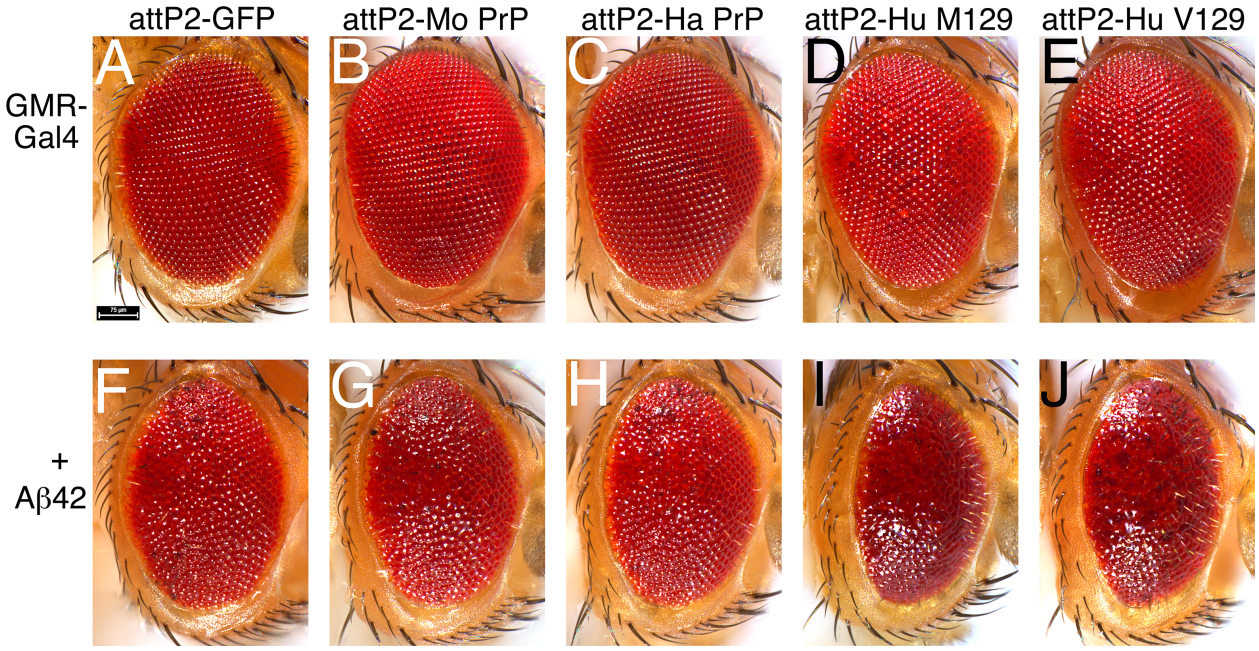

Fig. S3. Human PrP enhances the toxicity of Aβ42. A-J, Micrographs of fresh eyes expressing mCD8-GFP, hamster PrP, mouse PrP, human PrP-M129, or human PrP-V129 alone (A-E) or in combination with Aβ42 (F-J) in the eye under the control of *GMR-Gal4* at 25˚C. **A**, Control eyes from flies expressing mCD8-GFP (*GMR-Gal4 / UAS-mCD8-GFP-attP2*). **B and C**, Eyes from flies expressing mouse or hamster PrP (*GMR-Gal4 / UAS-mouse PrP-attP2 and GMR-Gal4 / UAS-hamster PrP-attP2*) are normal. **D and E**, Eyes from flies expressing human PrP (*GMR-Gal4 / UAS-human PrP-M129-attP2 and GMR-Gal4 / UAS-human PrP-V129-attP2*) show mild disorganization. These phenotypes are weak because the expression of PrP constructs is lower at 25˚C. **F**, The eyes from flies co-expressing GFP and Aβ42 (*GMR-Gal4 / UAS-mCD8-GFP-attP2/ UAS-Aβ42*) are disorganized and have necrotic spots. **G and H**, The eyes from flies co-expressing rodent PrP with Aβ42 (*GMR-Gal4 / UAS-mouse PrP-attP2 / UAS-Aβ42 and GMR-Gal4 / UAS-hamster PrP-attP2 / UAS-Aβ42*) are similar to those in F. **I and J**, The eyes from flies co-expressing human PrP and Aβ42 (*GMR-Gal4 / UAS-human PrP-M129-attP2 / UAS-Aβ42 and GMR-Gal4 / UAS-human PrP-V129-attP2 / UAS-Aβ42*) are smaller and highly disorganized (glassy).

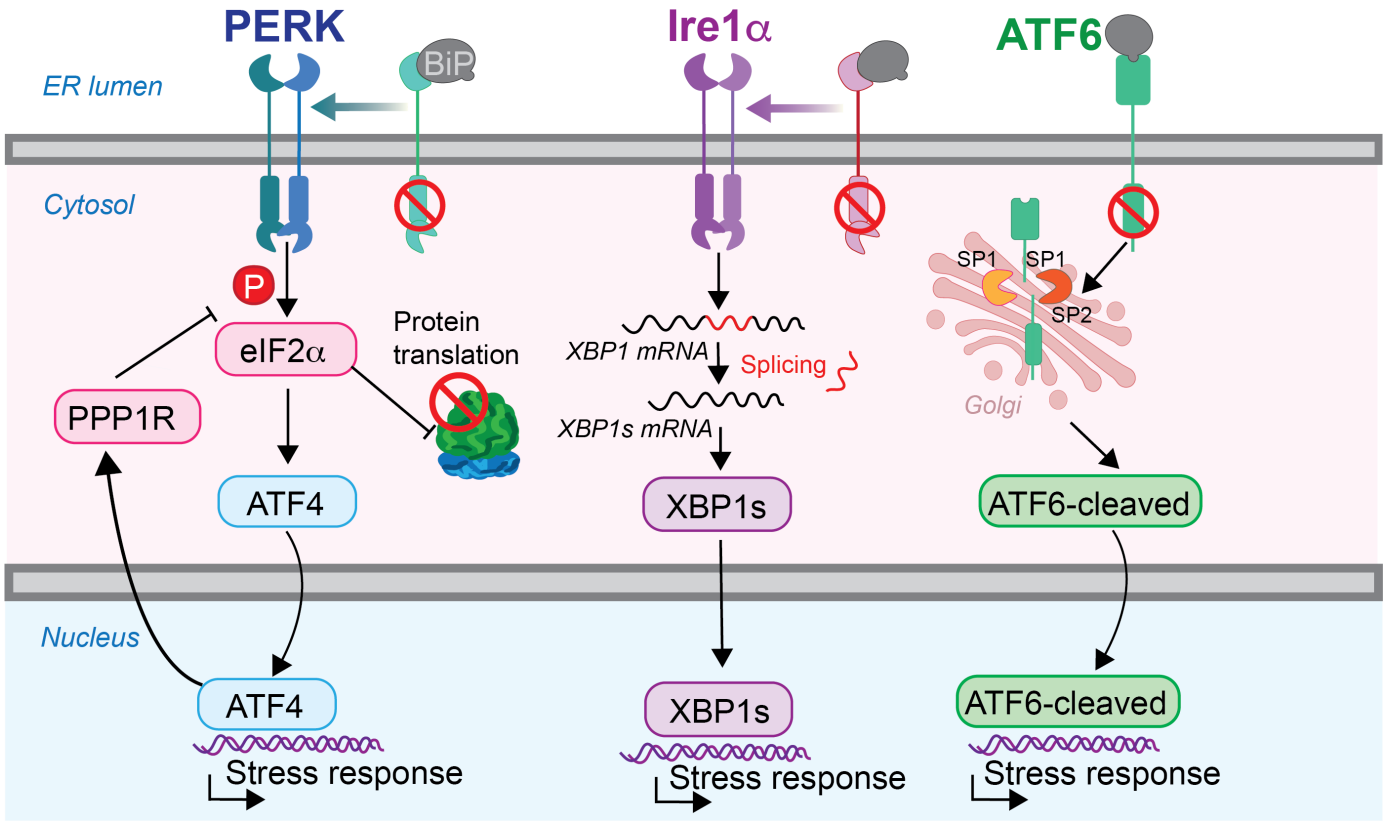

Fig. S4. Summary of the three UPR branches. PERK, Ire1 and ATF6 are three sensors of ER stress that are activated when the chaperone BiP releases the sensors due to an increase of misfolded proteins in the ER. Each sensor activates a different branch of the UPR consisting of different mechanisms of activation and downstream effectors. The overall consequence is acutely blocking translation and increasing the ER biosynthetic and folding capacities.

Table S1. Predicted age at specified climbing indices (α = 0.05).

Genotype	RU(+/-)	Climbing Index	Predicted Age (Days)	Std Error	Lower 0.95	Upper 0.95
HaPrP	-	90	1.09	1.27	-1.58	3.76
HaPrP	-	75	6.38	0.38	5.58	7.18
HaPrP	-	50	11.86	0.35	11.12	12.61
HaPrP	-	25	17.42	0.48	16.41	18.42
HaPrP	-	10	22.99	0.90	21.10	24.88
HaPrP	+	90	4.00	1.84	0.12	7.88
HaPrP	+	75	10.23	0.55	9.07	11.39
HaPrP	+	50	14.76	0.40	13.91	15.62
HaPrP	+	25	18.94	0.52	17.83	20.05
HaPrP	+	10	23.01	0.90	21.12	24.90
HuPrP	-	90	--	--	--	--
HuPrP	-	75	3.09	3.20	-3.66	9.85
HuPrP	-	50	15.47	0.44	14.54	16.40
HuPrP	-	25	20.99	0.43	20.07	21.90
HuPrP	-	10	25.77	0.78	24.13	27.41
HuPrP	+	90	0.72	0.03	0.64	0.79
HuPrP	+	75	0.87	0.03	0.81	0.93
HuPrP	+	50	1.21	0.02	1.16	1.26
HuPrP	+	25	1.80	0.05	1.69	1.91
HuPrP	+	10	2.56	0.10	2.35	2.77
LacZ	-	90	--	--	--	--
LacZ	-	75	3.68	1.13	1.30	6.07
LacZ	-	50	14.06	0.34	13.35	14.77
LacZ	-	25	20.16	0.35	19.43	20.90
LacZ	-	10	25.60	0.64	24.24	26.95
LacZ	+	90	--	--	--	--
LacZ	+	75	10.07	0.63	8.74	11.41
LacZ	+	50	16.36	0.43	15.44	17.27
LacZ	+	25	21.59	0.53	20.48	22.71
LacZ	+	10	26.56	0.94	24.58	28.53

Table S2. Climbing Index prediction formulas and parameters.

Prediction Model	Prediction formula	Genotype	RU(+/-)	θ1	q2	q3
3-parameter logistic	*Log((q1/ Climbing Index)/ q2)/ q3*	HaPrP	-	101.05	0.1	0.2
		HaPrP	+	94.19	0.02	0.27
		HuPrP	-	76.96	0.01	0.24
		LacZ	-	79.92	0.03	0.21
		LacZ	+	89.09	0.02	0.23
3-parameter 1st order decay kinetic	*Log((Climbing Index - q3)/ q1)/ (-q2)*	HuPrP	+	209.74	1.18	-0.3

Table S3. ANOVA analysis for XBP-GFP expression.

Comparisons for all pairs using Tukey-Kramer HSD

Connecting Letters Report

Level			Mean (Mean signal)	Mean (Integrated density)
Abeta42	A		12.749299	1298165.5
PrP-V129		B	10.634235	966270.2
Control		C	6.193575	540884.8

Levels not connected by same letter are significantly different.

Ordered Differences Report (mean signal)

Level	- Level	p-Value (mean signal)	p-Value (Integrated density)
Abeta42	Control	<.0001	<.0001
PrP-V129	Control	<.0001	0.0005
Abeta42	PrP-V129	0.0004	0.0008

Table S4. Summary of interactions with the UPR-PERK components

27˚C Stock#	**UAS-LacZ** 3955	**GD-Ire1αi** 39561	**TRiP-Ire1αi** 62156	**KK-XBP1i** 109312	**TRiP-XBP1i** 25990	**UAS-XBP1** 60730	**UAS-mXBP1s** Casas-Tinto 2011	**KK-PERKi** 110278	**TRiP-PERKi** 42499	**UAS-PERK** 76248
GMR	N0000	N0000	N0000	N0000	N0000	N0000	N0000	N0000	N0000	E3332
GMR PrP	E23000	E3311	E2201	E3300	E2300	N0000	N0000	S3300	S3300	E3332
	KK-ATF4i 109014	**TRiP-ATF4i** 25985	**UAS-ATF4** FlyORF	**UAS-ATF4** 81650	**TRiP-eIF2αi** 44449	**KK-eiF2αi** 104562	**KK-PPP1R15** 107545	**TRiP-PPP1R15** 33011	**TRiP-4E-BPi** 80427	**UAS-4E-BP** 9147
GMR	N0000	N0000	N0000	E1210	E1101	E0110	E0100	N0000	N0000	N0000
GMR PrP	S3300	S2200	N0000	E3332	E1312	E0210	L0003	L0003	S3300	E0110

Scoring: N-No effect; S: suppressor; E: enhancer; L: lethal. Effect scored 0 (no effect) – 3 (robust change) for: size-organization-pigmentation-lethality.

Table S5. Eye phenotypes of human PrP mutants

27˚C HuPrP	**UAS-CD8-GFP**	**V129 (WT)**	**N159D (dog)**	**D167S (horse)**	**N159D D167S-2x**	**N159D D167S, N174S-3x**
GMR	N0000	E1200	E1200	E0100	E01000	E0100

Scoring: N-No effect; S: suppressor; E: enhancer. Effect scored 0 (no effect) – 3 (robust change) for: size-organization-pigmentation-lethality.

Table S6. Two-wayANOVA analysis for mushroom bodies

Comparisons for all pairs using Tukey-Kramer HSD

Connecting Letters Report

Level					Mean
Control-D40	A				9888.5951
Control-D1		B			6754.0952
3X-D40			C		5530.1558
V129-D1			CD		5278.4658
2X-D1			CD		5246.9839
N159D-D1			CD		5102.4767
D167S-D1			CD		5046.6443
D167S-D40			CD		5022.8778
3X-D1			CD		4815.1017
2X-D40				D	4566.5551
N159D-D40				E	3179.4648
V129-D40				E	2471.1883

Levels not connected by the same letter are significantly different.

Ordered Differences Report: T-test corrected

Subject 1	Subject 2	P-value	Holm p-value (0.05)	Significant (Y/N)
Control, D1	2x, D1	0.0001	0.000746269	Y
Control, D1	3x, D1	0.0001	0.000769231	Y
Control, D40	2x,d40	0.0001	0.000806452	Y
Control, D40	3x, D40	0.0001	0.000833333	Y
Control, D40	Control, D1	0.0001	0.000847458	Y
D167S, D1	Control, D1	0.0001	0.000862069	Y
D167S, d40	Control, D40	0.0001	0.000909091	Y
N159D, D1	Control, D1	0.0001	0.000925926	Y
N159D, D40	2x, D40	0.0001	0.000980392	Y
N159D, D40	3x, D40	0.0001	0.001020408	Y
N159D, D40	Control, D40	0.0001	0.00106383	Y
N159D, D40	D167S, D40	0.0001	0.001111111	Y
N159D, D40	N159D, D1	0.0001	0.001136364	Y
V129, D1	Control, D1	0.0001	0.001162791	Y

V129, D40	2x, D40	0.0001	0.001282051	Y
V129, D40	3x, D40	0.0001	0.001351351	Y
V129, D40	Control, D40	0.0001	0.001428571	Y
V129, D40	D167S, D40	0.0001	0.001515152	Y
V129, D40	V129, D1	0.0001	0.001612903	Y
3x, D40	2x, D40	0.004	0.001666667	N
3x, D40	3x, D1	0.0071	0.001785714	N
V129, D40	N159D, D40	0.0282	0.001851852	N
D167S, D40	3x, D40	0.059	0.002	N
V129, D1	3x, D1	0.0663	0.002083333	N
D167S, D40	2x, D40	0.0821	0.002173913	N
3x, D1	2x, D1	0.0867	0.002272727	N
2x, D40	2x, D1	0.087	0.002380952	N
N159D, D1	3x, D1	0.2297	0.002941176	N
V129, D1	D167S, D1	0.4034	0.004545455	N
d167s, D1	3x, D1	0.404	0.005	N
V129, D1	N159D, D1	0.4612	0.00625	N
d167s, D1	2x, D1	0.4701	0.007142857	N
N159D, D1	2x, D1	0.545	0.008333333	N
N159D, D1	D167S, D1	0.8339	0.0125	N
V129, D1	2x, D1	0.9	0.016666667	N
D167S, D40	D167S, D1	0.9328	0.025	N